LATTICE QCD: CONCEPTS, TECHNIQUES AND SOME RESULTS*

Christian Hoelbling

Bergische Universität Wuppertal
Gausstrasse 20, 42119 Wuppertal, Germany

(Received November 4, 2014)

I give a brief introduction to lattice QCD for non-specialists.

DOI:10.5506/APhysPolB.45.2143
PACS numbers: 11.15.Ha, 12.38.Gc, 14.20.–c, 12.38.Mh

1. Introduction

Quantum chromodynamics (QCD) [1] is widely recognised as being the correct fundamental theory of the strong nuclear interaction. Its fundamental degrees of freedom are quarks and gluons, and their interactions at high energies are well described by perturbation theory because of asymptotic freedom [2, 3]. There is, however, a substantial discrepancy between these fundamental degrees of freedom and the asymptotic states of the theory, which are hadrons and their bound states. Since hadrons are thought of as strongly coupled bound states of quarks and gluons, it is obvious that a classical perturbative treatment is not sufficient to describe them from first principles.

Lattice gauge theory presents a framework in which to understand quantitatively this strongly coupled low energy sector of the theory from first principles. There are two main motivations for this: On the one hand, we would like to develop a full understanding of the dynamics of QCD itself and on the other hand, we would like to reliably subtract QCD contributions from observables designed to probe other fundamental physics. In this paper, I will explore the first of these two motives only. In Section 2, I will introduce lattice QCD, and give an overview of the techniques used in lattice QCD calculation in Section 3. In Section 4, I will discuss the determination of the ground state light hadron spectrum as an example of a lattice QCD calculation and in Section 5, I will briefly introduce finite temperature lattice QCD and highlight some important results.

* Invited talk presented at the LIV Cracow School of Theoretical Physics "QCD Meets Experiment", Zakopane, Poland, June 12–20, 2014.

I would like to emphasize that this paper is not intended to be a complete introduction to lattice QCD in any sense. The aim is rather to provide people working in related areas with a rough overview of lattice techniques, what they are able to provide today and what their limitations are. Consequently, details and proofs are often omitted and I refer the interested reader to the introductory literature on the subject for more in-depth coverage [4–12].

2. Formulation of lattice QCD

2.1. Continuum QCD

QCD is an SU(3) gauge theory with fermions in the fundamental representation. The Lagrangian of QCD is

$$\mathcal{L}_{\mathrm{QCD}} = -\tfrac{1}{4} G^a_{\mu\nu} G^{a\mu\nu} + \bar{\psi}\left(i D_\mu \gamma^\mu - m\right)\psi\,, \tag{1}$$

where the field strength tensor $G^a_{\mu\nu} = \partial_\mu A^a_\nu - \partial_\nu A^a_\mu + g f^{abc} A^b_\mu A^c_\nu$ with coupling g, the structure constants f^{abc} of SU(3) and the covariant derivative $D_\mu = \partial_\mu + g A^a_\mu \frac{\lambda^a}{2i}$ with λ^a denoting the Gell-Mann matrices. Both $\bar{\psi}$ and ψ carry an implicit flavour index and m is a $N \times N$ matrix in flavour space for N quark flavours.

A fundamental property of the QCD Lagrangian Eq. (1) is its invariance under a local SU(3) symmetry

$$\begin{aligned} \psi(x) &\to G(x)\psi(x)\,, \\ \bar{\psi}(x) &\to \bar{\psi}(x) G^\dagger(x)\,, \\ A_\mu(x) &\to G(x) A_\mu(x) G^\dagger(x) - \frac{i}{g}\left(\partial_\mu G(x)\right) G^\dagger(x) \end{aligned} \tag{2}$$

with $G(x) \in \mathrm{SU}(3)$ an arbitrary local gauge transformation. Since any physical quantity cannot depend on our arbitrary choice of a gauge, only gauge invariant quantities can be physical.

In addition to gauge symmetry, the QCD Lagrangian Eq. (1) has a global U(N) flavour symmetry

$$\begin{aligned} \psi(x) &\to e^{i\tau_a \phi}\psi(x)\,, \\ \bar{\psi}(x) &\to \bar{\psi}(x) e^{-i\tau_a \phi}\,, \end{aligned} \tag{3}$$

where the τ_a are the N^2 generators of U(N). In the case of vanishing quark mass $m = 0$, there is an additional chiral symmetry

$$\begin{aligned} \psi(x) &\to e^{i\tau_a \gamma_5 \phi}\psi(x)\,, \\ \bar{\psi}(x) &\to \bar{\psi}(x) e^{i\tau_a \gamma_5 \phi} \end{aligned} \tag{4}$$

whose diagonal part $\tau_a = \mathbb{1}$ is anomalous [13, 14], leaving an SU(N) symmetry intact.

We quantize QCD using the Feynman path integral formalism. We can express the expectation value of a time ordered product of operators as

$$\langle 0|T\Big(\hat{\mathcal{O}}_1(x_1)\dots\hat{\mathcal{O}}_n(x_n)\Big)|0\rangle = \frac{\int DA_\mu D\psi D\bar{\psi}\hat{\mathcal{O}}_1(x_1)\dots\hat{\mathcal{O}}_n(x_n)e^{i\hat{S}\left[A_\mu,\psi,\bar{\psi}\right]}}{\int DA_\mu D\psi D\bar{\psi}e^{i\hat{S}\left[A_\mu,\psi,\bar{\psi}\right]}}\,, \tag{5}$$

where we need to integrate over all fermion and gauge fields ψ, $\bar{\psi}$ and A_μ. The integral in Eq. (5) is not well defined unless we specify a regulator, which we will provide by discretizing the theory on a finite space-time lattice. Before we do so however, we perform another step: we analytically continue the integral in Eq. (5) to imaginary time, which is possible as long as the Hamiltonian of the theory is bounded from below. In the resulting Euclidean path integral

$$\langle 0|T(\mathcal{O}_1(x_1)\dots\mathcal{O}_n(x_n))|0\rangle = \frac{\int DA_\mu D\psi D\bar{\psi}\mathcal{O}_1(x_1)\dots\mathcal{O}_n(x_n)e^{-S\left[A_\mu,\psi,\bar{\psi}\right]}}{\int DA_\mu D\psi D\bar{\psi}e^{-S\left[A_\mu,\psi,\bar{\psi}\right]}} \tag{6}$$

with the Euclidean QCD action

$$\mathcal{S} = \int d^4x\left(\tfrac{1}{4}G^a_{\mu\nu}G^{a\mu\nu} + \bar{\psi}\left(iD_\mu\gamma^\mu + m\right)\psi\right) \tag{7}$$

the phase factor $e^{i\hat{S}}$ is replaced by a real valued exponential e^{-S}. Equation (6) can then be interpreted as the expectation value of the observable with respect to the positive definite measure $DA_\mu D\psi D\bar{\psi}e^{-S}$. It is interesting to note, that the r.h.s. of Eq. (6) can also be viewed as a thermodynamic expectation value with respect to a Boltzmann factor e^{-S}. It is, therefore, customary to call the denominator of Eq. (6) the partition function

$$\mathcal{Z} = \int DA_\mu D\psi D\bar{\psi}e^{-S\left[A_\mu,\psi,\bar{\psi}\right]}\,. \tag{8}$$

2.2. Lattice regularization

We now proceed to introduce a UV regularization of Euclidean QCD by discretizing the theory on a finite space-time lattice [15]. The lattice is hypercubic with a distance a between nearest neighbouring points (the lattice spacing). We also provide an IR regularization of the theory by a finite extent of the lattice in spatial $L = N_x a$ and temporal $T = N_t a$ directions and impose toroidal boundary conditions. As is the case for any other regularizations, we have to remove them eventually in order to obtain physical results. In lattice terminology, the process of removing the UV cutoff is known as the continuum limit, whereas the removal of the IR cutoff is the infinite volume limit.

Fermion fields $\psi(x)$ of the regularized theory are defined on the lattice sites x with $x_i \in a\{0,\ldots,N_x-1\}$ and $x_4 \in a\{0,\ldots,N_t-1\}$. In order to preserve exact gauge invariance, gauge fields are treated differently however. Instead of discretizing the gauge potential at each lattice site $A_\mu(x)$ directly, we discretize the parallel transport between any site and its nearest neighbours. In QCD, one typically uses the group element $U_\mu(x)$ directly, where it is understood that this represents the continuum parallel transport

$$U_\mu(x) = \mathcal{P} e^{ig\int_x^{x+e_\mu} dz_\mu A_\mu(z)}\,, \tag{9}$$

where $\mathcal{P}$ denotes the path ordered product and e_μ is the vector of length a in μ direction. The reverse parallel transport is then given by

$$U_{-\mu}(x) = \mathcal{P} e^{ig\int_x^{x-e_\mu} dz_\mu A_\mu(z)} = U_\mu^\dagger(x-e_\mu)\,. \tag{10}$$

With these definitions and the gauge transformations Eq. (2), we find that the lattice fields transform as

$$\begin{aligned} \psi(x) &\to G(x)\psi(x)\,,\\ \bar\psi(x) &\to \bar\psi(x)G^\dagger(x)\,,\\ U_\mu(x) &\to G(x)U_\mu(x)G^\dagger(x+e_\mu)\,. \end{aligned} \tag{11}$$

In order to proceed, we need to construct gauge invariant quantities from our lattice fields. We will need them for two distinct purposes: First, we want to construct a lattice action and second, we need to find gauge invariant observables. In principle, we have two choices of constructing gauge invariant objects (see Fig. 1). We can either take traces of closed loops of parallel transports (gauge links) $\mathrm{Tr}(U_{\mu_1}(x)U_{\mu_2}(x+e_{\mu_1})\ldots U_{\mu_n}^\dagger(x))$ or we can take a fermion–antifermion pair that is connected by gauge links $\bar\psi(x)U_{\mu_1}\ldots U_{\mu_n}^\dagger(y)\psi(y)$.

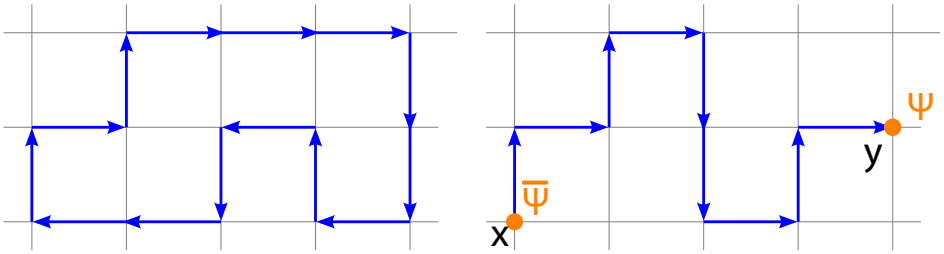

Fig. 1. Two possibilities of constructing a gauge invariant object in a lattice gauge theory. Left: A closed loop of parallel transports (gauge links). Right: A fermion and an antifermion connected by gauge links.

The simplest[1] object we can construct of gauge links alone is called the plaquette (see Fig. 2). It is defined as the trace of the path ordered product of gauge links around an elementary square in the μ–ν plane

$$P_{\mu\nu}(x) = \mathrm{Tr}\left(U_\mu(x)U_\nu(x+e_\mu)U_\mu^\dagger(x+e_\nu)U_\nu^\dagger(x)\right) . \tag{12}$$

Using Eq. (9), we can express the plaquette in terms of continuum gauge potentials. Taylor expanding in the lattice spacing a results in

$$P_{\mu\nu}(x) = \mathrm{Tr}\left(1 + iga^2 G_{\mu\nu}(x) - \frac{g^2a^4}{2}G_{\mu\nu}^2(x)\right) + \mathcal{O}\left(g^6\right) . \tag{13}$$

We can use this result to construct a gauge action

$$S_G = \beta \sum_{x,\mu>\nu} \left(1 - \tfrac{1}{6}\left(P_{\mu\nu}(x) + P_{\mu\nu}^\dagger(x)\right)\right) \tag{14}$$

with $\beta = 6/g^2$ that has the correct form in the continuum limit

$$S_G \overset{a\to 0}{\longrightarrow} \frac{1}{4}\int d^4x G_{\mu\nu}^a(x)G_{\mu\nu}^a(x) . \tag{15}$$

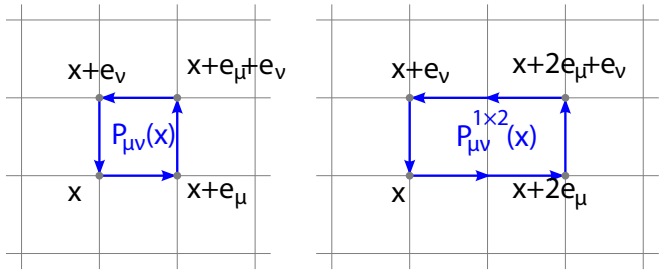

Fig. 2. An elementary plaquette (left) and an extended 2×1 Wilson loop (right).

The gauge action Eq. (14) is known as the Wilson plaquette action. It has the correct continuum limit with leading corrections of $\mathcal{O}(a^2)$. It is not the only possible discretization of the continuum gauge action Eq. (7) though. One could equally well take *e.g.* a trace $W_{\mu\nu}^{2\times1}$ over a closed loop of gauge links around a 2×1 rectangle (see Fig. 2). This object, known as

[1] Since the lattice has a torus topology, it is possible to construct closed gauge loops that wind around any direction. This object is called Wilson line or Polyakov loop. Therefore, it is possible on lattices with an extent of 3 or fewer lattice spacings in one direction to construct a gauge invariant object entirely consisting of even fewer gauge links.

the Wilson loop of size 2×1, has the same leading continuum behaviour as the plaquette up to a trivial numerical factor. One could therefore, in principle, use it instead of the plaquette for defining a lattice gauge action, which, however, is not particularly useful. What is useful, however, is taking a linear combination of the elementary plaquette and the 2×1 Wilson loop [16–18]. Choosing the relative weights such that the leading order term in the continuum limit remains unchanged, while the leading corrections of $\mathcal{O}(a^2)$ (which have the same form for both terms) cancel, we obtain an action that has leading corrections of $\mathcal{O}(a^4)$ only. Classically, these coefficients are easy to find. They can be read off from a Taylor expansion of the lattice operators in terms of continuum operators. The resulting action

$$S_G = \beta \sum_{x,\mu>\nu} \left(1 - \tfrac{1}{6}\left(\tfrac{5}{3}P_{\mu\nu}(x) - \tfrac{1}{12}W^{2\times1}_{\mu\nu}(x)\right) + \text{h.c.}\right) \tag{16}$$

is known as the tree-level Lüscher–Weisz action. In a quantum theory, there are radiative corrections and one can, in principle, determine the relative weights by either computing them in perturbation theory or finding them nonperturbatively [19–22].

This construction of a gauge action that has higher order cutoff terms is a special case of the Symanzik improvement program [23, 24]. Generically, the idea behind it is that the lattice theory, as an effective theory with a finite cutoff, may contain continuum irrelevant, nonrenormalizable terms without altering the continuum limit. One can thus perform an expansion of the continuum action in terms of lattice operators. The nontrivial part of this expansion are the kinetic terms where continuum derivative operators are expanded in discrete difference operators. As an illustrative example, let us consider the classical expansion of the simple derivative operator

$$\frac{d}{dx}f(x) = f'(x)\,. \tag{17}$$

On a discrete set of points with uniform spacing a, we can define a sequence of finite difference operators

$$\Delta_n f(x) := \frac{f(x+na) - f(x-na)}{2na}\,. \tag{18}$$

Taylor expanding this expression around x one obtains

$$\Delta_n f(x) = \sum_{i=0}^{\infty} \frac{(na)^{2i}}{(2i+1)!} f^{(2i+1)}(x) = f'(x) + \frac{1}{6}(na)^2 f'''(x) + \mathcal{O}\left(a^4\right) \tag{19}$$

and thus the finite difference operator

$$\Delta f(x) := \left(\tfrac{4}{3}\Delta_1 - \tfrac{1}{3}\Delta_2\right) f(x) \tag{20}$$

has classical discretization errors

$$\Delta f(x) = f'(x) + \mathcal{O}\left(a^4\right) . \tag{21}$$

2.3. Fermion discretization

In the Euclidean continuum theory, the free fermion action reads

$$S_F = \int d^4x \bar{\psi}(x) \left(\gamma_\mu \partial_\mu + m\right) \psi(x) . \tag{22}$$

The most straightforward discretization of this action is

$$S_F^N = a^4 \sum_x \bar{\psi}(x) \left(\gamma_\mu \Delta_\mu + m\right) \psi(x) \tag{23}$$

with the simple difference operator

$$\Delta_\mu f(x) := \frac{f(x + e_\mu) - f(x - e_\mu)}{2a} . \tag{24}$$

We can diagonalize this operator in Fourier space. The resulting inverse propagator has the form

$$G_N^{-1}(p) = i\gamma_\mu \frac{\sin ap_\mu}{a} + m . \tag{25}$$

Performing the continuum limit $a \to 0$ for a *fixed physical momentum* p_μ, we recover the continuum inverse propagator

$$G_N^{-1}(p) \stackrel{a\to 0}{\longrightarrow} i\gamma_\mu p_\mu + m \tag{26}$$

which has the correct physical poles at $p^2 = -m^2$. Lattice periodicity requires that these poles are repeated for $p_\mu \to p_\mu + 2\pi/a$, but Eq. (26) has additional poles within the Brillouin zone for $p_\mu \to p_\mu + \pi/a$. In addition to the physical pole, there are $2^D - 1$ of these doubler fermion poles within the Brillouin zone, so in $4D$ the naive fermion action Eq. (23) does, in fact, describe 16 species of fermions instead of one.

This feature is known as the fermion doubling problem. It is not specific to the naive fermion action, as can be seen from the following heuristic argument. Let us try to generalize the action and, therefore, the inverse propagator Eq. (25). We may replace $\sin(ap_\mu)/a$ with a generic function $P_\mu(ap_\mu)/a$. Around $ap_\mu = 0$, $P_\mu(ap_\mu) = ap_\mu + \mathcal{O}(a^2)$ is dictated by the requirement of correct behaviour of physical modes in the continuum limit (Eq. (26)). Similarly, lattice periodicity requires that $P_\mu(ap_\mu + 2\pi) = ap_\mu + \mathcal{O}(a^2)$. One

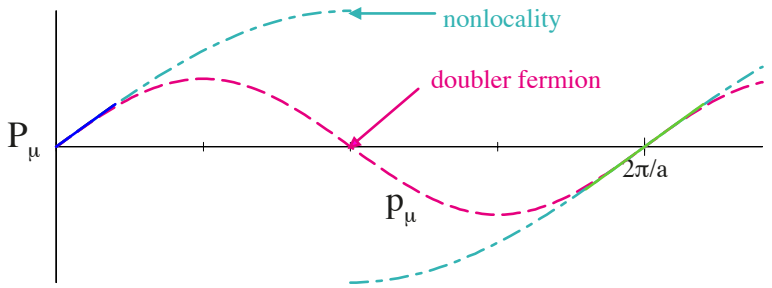

Fig. 3. Illustration of the possible behaviours of $P_\mu(ap_\mu)$.

can, therefore, have an additional zero crossing of $P_\mu(ap_\mu)$ within the Brillouin zone or a discontinuity of the function. The former corresponds to a doubler mode while the later, in coordinate space, corresponds to a nonlocal operator. This situation is depicted in Fig. 3.

Of course, replacing $\sin(ap_\mu)/a$ by $P_\mu(ap_\mu)/a$ in Eq. (25) is not the most generic ansatz. One could try to add a term to the action that vanishes at $ap_\mu = 0$ but gives a large contribution at the doubler momenta. If we require, in addition, that the chiral symmetry of the continuum action Eq. (4) is respected by the lattice action, our choices are severely restricted. Continuum chiral symmetry requires the additional term to anticommute with γ_5, so the only other term we may add has the form $\gamma_\mu\gamma_5 R_\mu(ap_\mu)$. For a correct continuum limit, this term has to vanish at $ap_\mu = 2\pi n$, too. A possible action along these lines would be

$$S_F = a^4 \sum_x \bar{\psi}(x) \left(\gamma_\mu \Delta_\mu + a\gamma_\mu\gamma_5 \Box_\mu + m\right) \psi(x) \tag{27}$$

with

$$\Box_\mu f(x) := \frac{f(x+e_\mu) - 2f(x) + f(x-e_\mu)}{2a^2} \tag{28}$$

which would lead to an inverse propagator

$$G^{-1}(p) = i\gamma_\mu \frac{\sin ap_\mu}{a} + \gamma_\mu\gamma_5 \frac{1-\cos ap_\mu}{a} + m\,. \tag{29}$$

One can check that the effect of the additional term in Eq. (29) is just to shift the doubler poles within the Brillouin zone. The only other possibility that is left, namely adding cross-terms, will have a similar effect of shifting the doubler poles within the multidimensional Brillouin zone. There is, in fact, a no-go theorem by Nielsen and Ninomiya [25–27] that states the impossibility of a fermion discretization that simultaneously fulfils all of the following requirements:

1. The absence of doubler modes.
2. Invariance under continuum chiral symmetry.
3. Locality of the fermion operator.
4. The correct continuum limit.

It was also pointed out by Karsten and Smit [28] that the emergence of doubler modes for lattice fermions is a natural consequence of the general feature that a regulated theory is anomaly free. The chiral anomaly of the physical mode is cancelled by the anomaly of the doubler modes[2].

In order to proceed, we therefore need to throw one of the desired features of our fermion action overboard. Since we cannot really sacrifice the correct continuum limit or the locality of the operator, the choices are to either violate continuum chiral symmetry or to live with some doubler fermions. The former is most easily accomplished by adding a term to the action that is very similar in spirit to Eq. (27) but violates chiral symmetry (Eq. (4)). The resulting action [31]

$$S_F^{\mathrm{W}} = a^4 \sum_x \bar{\psi}(x) \left(\gamma_\mu \Delta_\mu + ra\Box + m\right) \psi(x) \tag{30}$$

is known as the Wilson fermion action, where we have used $\Box = \sum_\mu \Box_\mu$. The Wilson parameter r is usually set to $r = 1$. Fourier transforming to momentum space, we can read off the inverse propagator as

$$G^{-1}(p) = i\gamma_\mu \frac{\sin ap_\mu}{a} + \sum_\mu \frac{1 - \cos ap_\mu}{a} + m\,. \tag{31}$$

We can see that although the Wilson term in Eq. (30) is formally suppressed by a in the continuum limit, it does very different things to physical and doubler modes. At fixed *physical* momentum p, the additional term in Eq. (31) vanishes indeed $\propto a$, while at fixed *lattice* momentum ap it gives a divergent contribution $\propto 1/a$. Notice also that while the naive term spreads the momenta into the imaginary direction, the Wilson term spreads them into the real one (*cf.* Fig. 4).

Introducing gluon fields in a gauge invariant manner is straightforward. We replace the finite difference operator by the covariant one

$$\Delta_\mu f(x) := \frac{U_\mu(x) f(x + e_\mu) - U_\mu^\dagger(x - e_\mu) f(x - e_\mu)}{2a} \tag{32}$$

[2] See also [29, 30].

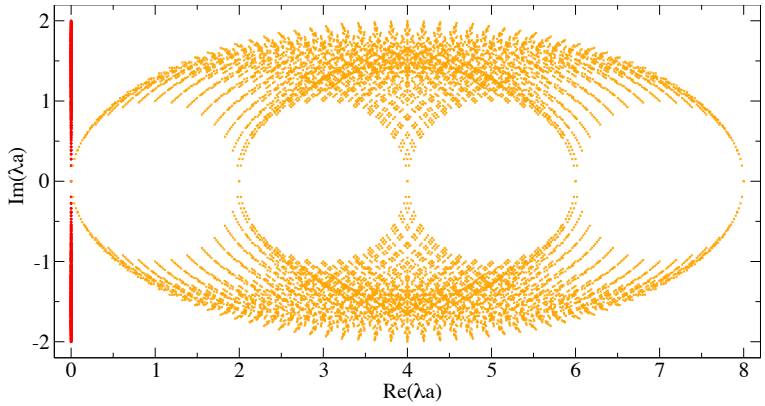

Fig. 4. Eigenvalue spectra of the free naive fermion operator (Eq. (26), along the imaginary axis) and the free Wilson fermion operator (Eq. (31), spread into the real direction) for $m = 0$ on a 32^4 lattice. The naive operator has a 16-fold degeneracy in each mode. Note that the spectrum of the free staggered fermion operator Eq. (42) is identical to the naive one except for the degeneracy, which is reduced by a factor of 4.

and the discretized second derivative by the covariant

$$\Box_\mu f(x) := \frac{U_\mu(x) f(x+e_\mu) - 2f(x) + U_\mu^\dagger(x-e_\mu) f(x-e_\mu)}{2a^2}\,. \tag{33}$$

Unlike the operator of the naive fermion action Eq. (23), the operator

$$D_{\mathrm{W}}(m) = \gamma_\mu \Delta_\mu + ra\Box + m \tag{34}$$

of the Wilson action Eq. (30) is no more antihermitian at $m = 0$. It does, however, fulfil the property

$$\gamma_5 D_{\mathrm{W}}(m) = D_{\mathrm{W}}^\dagger(m)\gamma_5 \tag{35}$$

which is known as γ_5-hermiticity. It implies that the eigenvalues of $D_{\mathrm{W}}(m)$ are either real or appear in complex conjugate pairs. This property renders the determinant of the operator real, which will be important for its numerical treatment. In addition, Eq. (35) implies that the left eigenvector of a complex mode $|i\rangle$ is related to the right eigenvector of the complex conjugate mode $|\hat{i}^*\rangle$ by $|\hat{i}^*\rangle = \gamma_5|i\rangle$ and the left and right eigenvectors $|j\rangle$ and $|\hat{j}\rangle$ of a real mode are related by $|\hat{j}\rangle = \gamma_5|j\rangle$. The latter property is the remnant of the chirality of zero modes of the continuum operator [32]. For a normal operator (*i.e.* when $|\hat{j}\rangle = |j\rangle$), it reads $|j\rangle = \gamma_5|j\rangle$.

Because of the explicit breaking of chiral symmetry, some additional operator mixing occurs in Wilson fermions that is absent in fermion formulations which respect chiral symmetry. As a consequence, Wilson fermions show some deficiencies, most notably an additive mass renormalization and a bad $\mathcal{O}(a)$ scaling behaviour. As in the case of gauge actions, these deficiencies can be ameliorated by following a Symanzik improvement program.

The most straightforward idea of constructing a Wilson-like operator with an improved continuum behaviour is including next-to-nearest neighbour points into the derivative terms similar to Eq. (20). Such an operator has been proposed by Hamber and Wu [33], but it is not used because a simpler alternative exists. Sheikholeslami and Wohlert [34] demonstrated that $\mathcal{O}(a)$ improvement can also be achieved by adding a Pauli term to the Wilson operator (Eq. (34))

$$D_{\mathrm{SW}} = D_{\mathrm{W}}(m) - a\frac{r c_{\mathrm{SW}}}{2}\sigma_{\mu\nu}G_{\mu\nu}\,. \tag{36}$$

From Eq. (13), we see that the value of the gluon field at the center of the plaquette can be obtained simply by taking the imaginary part of $P_{\mu\nu}$. In order to obtain it at a lattice site, the average over the four adjacent plaquettes is usually taken and the term is often referred to as the clover term.

The clover term in Eq. (36) comes with a coefficient c_{SW}. For classical or tree-level improvement, $c_{\mathrm{SW}} = 1$ and the resulting action has discretization effects of $\mathcal{O}(a^2)$ classically and $\mathcal{O}(\alpha_{\mathrm{s}}a)$ through quantum corrections. One can compute the quantum corrections either perturbatively [35, 36] or nonperturbatively [37], but the combination of tree-level clover improvement with UV-filtering (or smearing) techniques that will be discussed in Sect. 2.5 provides for a very efficient reduction of the $\mathcal{O}(\alpha_{\mathrm{s}}a)$ effects [38].

We now turn towards the second option for evading the Nielsen–Ninomiya theorem: living with doubler fermions. We saw that the naive fermion action Eq. (23) describes a theory with $2^D = 16$ poles in the fermion propagator. The poles are located such that one can reach another pole by adding/subtracting a momentum π/a to any momentum component p_μ. If one then starts from the pole at $p = 0$ and defines $p'_\mu = -(p_\mu \pm \pi/a)$, it is evident that the pole at $p_\mu = \pm\pi/a$ can be reinterpreted as the physical one in the new momenta. Note that due to the sign flip between the momenta definitions, chirality will be reversed when going to an adjacent pole.

In the free theory, there is an exact degeneracy between the fermions described by each of the 16 poles. In the interacting theory, high momentum gluons with momentum $\sim \pi/a$ will couple the different species. As the necessary momentum diverges for $a \to 0$, one can expect these mixing effects to disappear in the continuum limit. We will see later that there can be subtle order of limits effects however.

The general strategy of living with doubler fermions is now to project to one of the fermion species and suppress the effect of the others as much as possible. It has been noted very early on in the development of lattice gauge theory [39–41] that the naive fermion operator has an exact fourfold degeneracy even in the interacting case that can be exposed and lifted by a simple transformation. We start with the explicit form of the naive fermion action Eq. (23) in the interacting case

$$S_N = a^4 \sum_x \bar{\psi}(x)\gamma_\mu \frac{U_\mu(x)\psi(x+e_\mu) - U_\mu^\dagger(x-e_\mu)\psi(x-e_\mu)}{2a} + m\bar{\psi}(x)\psi(x)\,. \tag{37}$$

Substituting for the fermion fields

$$\psi(x) = \gamma_0^{\frac{x_0}{a}} \gamma_1^{\frac{x_1}{a}} \gamma_2^{\frac{x_2}{a}} \gamma_3^{\frac{x_3}{a}} \chi(x)\,, \tag{38}$$

$$\bar{\psi}(x) = \bar{\chi}(x)\gamma_3^{\frac{x_3}{a}} \gamma_2^{\frac{x_2}{a}} \gamma_1^{\frac{x_1}{a}} \gamma_0^{\frac{x_0}{a}}\,, \tag{39}$$

we obtain

$$S_{\mathrm{st}} = a^4 \sum_x \bar{\chi}(x)\eta_\mu(x) \frac{U_\mu(x)\chi(x+e_\mu) - U_\mu^\dagger(x-e_\mu)\chi(x-e_\mu)}{2a} + m\bar{\chi}(x)\chi(x)\,, \tag{40}$$

where $\eta_\mu(x)$ is a purely numerical factor

$$\eta_\mu(x) = (-1)^{\sum_{\nu<\mu} x_\nu}\,. \tag{41}$$

The corresponding staggered fermion operator reads

$$D_{\mathrm{st}}(m) = \eta_\mu \Delta_\mu + m\,. \tag{42}$$

We can, therefore, take $\bar{\chi}$ and χ to be single component fields, which lifts a fourfold exact degeneracy. The individual spinor components of the fermion field are not all present at each lattice site anymore. We can, however, infer from the transformation Eqs. (38)–(39) how to combine the 16 components present in an elementary hypercube into 4 species (or tastes) of 4-component fermion spinors. As the components of the fermion field are staggered across the lattice, the action is referred to as staggered fermions.

Staggered fermions satisfy an equivalent of γ_5-hermiticity Eq. (35)

$$\eta_5 D_{\mathrm{st}}(m) = D_{\mathrm{st}}^\dagger(m)\eta_5 \tag{43}$$

with

$$\eta_5(x) = (-1)^{x_0+x_1+x_2+x_3}\,. \tag{44}$$

They also retain a remnant of chiral symmetry at zero mass

$$\{D_{\mathrm{st}}(0), \eta_5\} = 0 \tag{45}$$

which implies cutoff terms of $\mathcal{O}(a^2)$ and the absence of additive mass renormalization. The symmetry Eq. (45) is, however, very different from the full continuum chiral symmetry. It is a U(1) and will be present, even if we want to describe a single fermion flavour which in the continuum does not have a chiral symmetry. The implications of this are discussed extensively in the literature [42–68] and while no definitive conclusion has been reached, there are many indications that staggered fermions do correctly reproduce the chiral symmetry pattern including the anomaly if an appropriate continuum limit is taken before going to the chiral limit.

A great number of additional fermion discretizations have been suggested in the literature and are used to some degree in recent lattice calculations. Among those are twisted mass fermions [69], which feature an improved scaling behaviour at the expense of flavour breaking, minimally doubled fermions [70–73] with only a single doubler pole that comes at the expense of breaking the lattice rotational symmetry or staggered fermions with an additional Wilson term to remove doubler modes from the physical spectrum [74–76]. The most numerous group, however, are fermion formulations that to some degree build upon the advances in understanding of chiral symmetry on the lattice.

2.4. Lattice chiral symmetry

The Nielsen–Ninomiya theorem seems to forbid the existence of an otherwise well-behaved lattice fermion with chiral symmetry. Its definition of chiral symmetry, however, is the continuum form. It demands that the fermion operator D anticommutes with γ_5, so $\gamma_5 D + D\gamma_5 = 0$. It has been realized very early on by Ginsparg and Wilson [77] that upon blocking from the continuum, the continuum chiral symmetry is replaced by the relation

$$\gamma_5 D + D\gamma_5 = \frac{a}{\rho} D\gamma_5 D\,. \tag{46}$$

Independently of this work, a class of lattice actions was constructed [78–80] by blocking transformations and it was realized that they fulfil the Ginsparg–Wilson relation Eq. (46) [81]. Another lattice fermion formulation was inspired by the discovery that in a 5-dimensional theory,S chiral fermions naturally arise along a 4-dimensional defect [82, 83] even on a lattice with finite cutoff [84]. The resulting domain wall fermion action [85] is still widely used today. Along similar lines, Narayanan and Neuberger developed the overlap fermion action [86–89], which was condensed into a

4-dimensional fermion operator by Neuberger [90]. This operator fulfils the Ginsparg–Wilson relation (Eq. (46)) [91] and in the massless case is given by

$$D_{\mathrm{ov}} = \frac{\rho}{a}\left(\mathbb{1} + \frac{D_{\mathrm{W}}(-\rho/a)}{\sqrt{D_{\mathrm{W}}^{\dagger}(-\rho/a)D_{\mathrm{W}}(-\rho/a)}}\right), \tag{47}$$

where $D_{\mathrm{W}}(-\rho/a)$ is the Wilson operator (Eq. (34)) at a negative bare mass $-\rho/a$. Note that the overlap operator also fulfils γ_5-hermiticity $\gamma_5 D_{\mathrm{ov}} = D_{\mathrm{ov}}^{\dagger}\gamma_5$.

Although the Ginsparg–Wilson relation is sometimes referred to as a minimal way of breaking chiral symmetry, it is, in fact, the correct chiral symmetry relation of the regulated theory [92]. This is somewhat more apparent after a trivial rewriting of Eq. (46)

$$\gamma_5 D + D\hat{\gamma}_5 = 0\,, \qquad \hat{\gamma}_5 = \gamma_5\left(1 - \frac{a}{\rho}D\right). \tag{48}$$

It implies that the fermion action

$$S = \bar{\psi}D\psi \tag{49}$$

is invariant under an infinitesimal chiral transformation

$$\bar{\psi} \to \bar{\psi}(\mathbb{1} + i\epsilon\gamma_5)\,, \qquad \psi \to (\mathbb{1} + i\epsilon\hat{\gamma}_5)\psi \tag{50}$$

which acts differently on the fermion and antifermion fields. Note, however, that Eq. (48) implies that in the continuum limit, the continuum form of chiral symmetry is restored

$$\hat{\gamma}_5 = \gamma_5\left(1 - \frac{a}{\rho}D\right) \overset{a\to 0}{\longrightarrow} \gamma_5\,. \tag{51}$$

Together with γ_5 hermiticity, $D\gamma_5 = \gamma_5 D$ the Ginsparg–Wilson relation Eq. (46) implies

$$D^{\dagger} + D = \frac{a}{\rho}DD^{\dagger} \tag{52}$$

which means that $\frac{a}{\rho}D - 1$ is a unitary operator and the eigenvalues of D lie on a circle of radius ρ/a touching the imaginary axis at the origin (see Fig. 5). The real modes of D are, therefore, located at either 0 or $2\rho/a$ and it can easily be shown that they are chiral. The modes at $2\rho/a$ correspond to all unphysical doubler branches and they can, in fact, be removed by a simple transformation of the fermion fields

$$\tilde{\psi} = \tilde{\mathbb{1}}\psi\,, \qquad \tilde{\mathbb{1}} = \mathbb{1} - \frac{a}{2\rho}D\,. \tag{53}$$

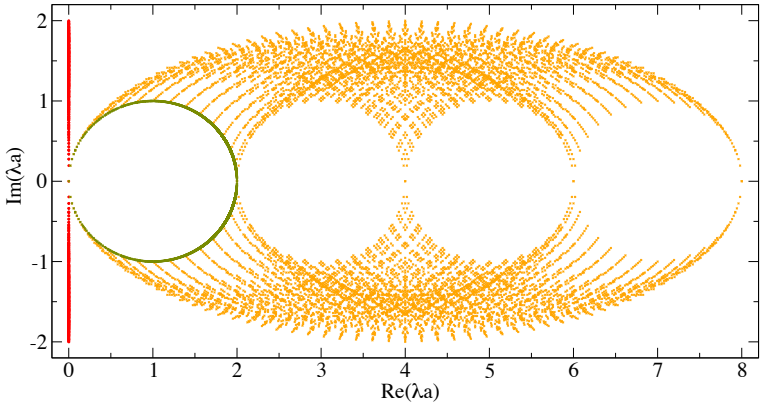

Fig. 5. Eigenvalue spectrum of the free overlap operator with $\rho = 1$ (Eq. (47), circle) compared to the free Wilson (Eq. (31), spread into the real direction) and staggered (Eq. (42), along the imaginary axis) operators on a 32^4 lattice.

The (massless) fermion action can now be written as

$$S = \bar{\psi} \frac{D}{1 - \frac{a}{2\rho} D} \tilde{\psi} \tag{54}$$

which is an antihermitian operator. The chiral modes are at the origin and the doublers have been removed off to infinity. In fact, in the new field variables, the action now obeys the continuum form of chiral symmetry, *i.e.* it is invariant under

$$\bar{\psi} \to \bar{\psi}(\mathbb{1} + i\epsilon\gamma_5)\,, \qquad \tilde{\psi} \to (\mathbb{1} + i\epsilon\gamma_5)\tilde{\psi}\,. \tag{55}$$

All consequences of chiral symmetry, such as conserved axial currents, the correct anomaly, the absence of additive mass renormalization and discretization effects that start at $\mathcal{O}(a^2)$ are only, therefore, present for Ginsparg–Wilson fermions provided that the correctly rotated field variables are used for constructing the observables. One can now also add a mass term to Ginsparg–Wilson fermions that behaves exactly like a continuum mass term

$$D(m) = D + \tilde{\mathbb{1}} m\,. \tag{56}$$

The main disadvantage of chirally symmetric fermions for numerical computations is their cost. Simple fermion discretizations, such as the Wilson or staggered ones, typically have fermion operators with a limited number of couplings to neighbour sites. Numerically, this translates into them being sparse matrices. In contrast, chirally symmetric operators, such as *e.g.* the

overlap operator Eq. (47), tend to be full matrices which are much more demanding computationally. In fact, there is a theorem [93, 94] that chirally symmetric operators cannot be realized with a finite number of couplings to their nearest neighbours in four dimensions, a property that is referred to as ultralocality in the lattice literature. One can still have an ultralocal chiral fermion operator if one includes an extra fifth dimension as is done in the case of domain wall fermions. The price to pay there, however, is that the extent of the fifth dimension has to be made infinitely large, in principle, to have exact chiral symmetry. Obviously, this strategy implies considerable additional computational effort, too.

2.5. Effects of UV modes

It is evident from Fig. 5 that the physical modes of a lattice fermion operator which are located around the origin are by far outnumbered by UV modes. Modes that are close to the cutoff do not carry a lot of physical information in the interacting case though. With increasing cutoff, these modes are ever deeper in the perturbative regime that is dominated by asymptotic freedom and their fluctuations mainly contribute towards enlarging cutoff effects.

It is possible to eliminate a large part of these fluctuations by a simple modification of the fermion operator. Remember that gauge interactions were introduced into the lattice theory by the covariant derivative (Eq. (32)) which contains the parallel transport $U_\mu(x)$ between the lattice points x and $x + e_\mu$. Note that we have chosen the gauge connection $U_\mu(x)$ along the minimal path connecting the two neighbouring points. Although this choice seems reasonable, it is not unique. In principle, one can choose any path connecting the two sites (see Fig. 6).

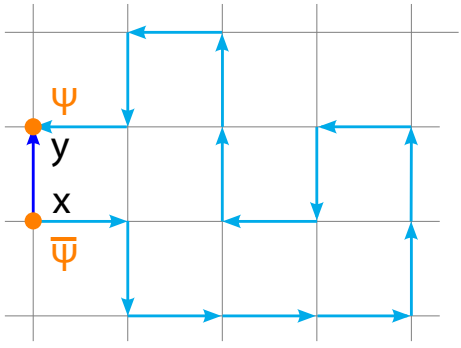

Fig. 6. Illustration of two different lattice paths, one of them minimal, between neighbouring points x and y.

This ambiguity can be used to effectively damp the coupling of gluons with momenta close to the cutoff to the fermions. The procedure is generically termed smearing, link fattening or UV-filtering and the first instance was proposed by the APE Collaboration [95]. In the APE smearing recipe, a fat or smeared gauge link $U_\mu^{(\mathrm{APE})}(x)$ in D dimensions is defined as a weighted average

$$U_\mu^{(\mathrm{APE})}(x) = (\alpha - 1)U_\mu(x) + \frac{\alpha}{2(D-1)}\Omega_\mu(x)\,, \tag{57}$$

where

$$\Omega_\mu(x) = \sum_{\mu\neq\mu} U_\nu(x)U_\mu(x+e_\nu)U_\nu^\dagger(x+e_\mu) + U_\nu^\dagger(x-e_\nu)U_\mu(x-e_\nu)U_\nu(x-e_\nu+e_\mu) \tag{58}$$

is the sum over staples (see Fig. 7) with the smearing parameter α typically chosen to be $\alpha \sim 0.6$. The smeared link $U_\mu^{(\mathrm{APE})}(x)$ can then be used in the fermion operator instead of the original "thin link" $U_\mu(x)$. For sufficiently smooth gauge configurations, *i.e.* for gauge configurations where the gluonic fields do not carry substantial momenta components at the cutoff scale, the difference between thin links and staples is irrelevant in the continuum limit. Consequently, the continuum limit is not affected by replacing thin links with smeared ones in the fermionic operator.

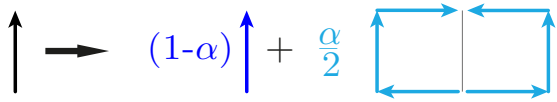

Fig. 7. Illustration of the APE smearing procedure [95] in the 2-dimensional case. The link connecting nearest neighbouring sites in the fermion operator is replaced by a weighted average of the "thin link" (weight $1-\alpha$) and the "staple" (weight $\alpha/2(D-1)$).

This simple recipe has a shortcoming though. The new link variable $U_\mu^{(\mathrm{APE})}(x)$ was obtained by averaging elements of the gauge group and, therefore, is not, in general, an element of the gauge group itself. This can be remedied by a simple unitary backprojection

$$U' = \frac{U^{(\mathrm{APE})}}{\sqrt{U^{(\mathrm{APE})^\dagger}U^{(\mathrm{APE})}}} \tag{59}$$

followed by dividing out the phase of the determinant

$$\hat{U} = \frac{U'}{(\det(U'))^{1/3}}\,. \tag{60}$$

This procedure is continuum irrelevant on sufficiently smooth gauge fields, too. One can, therefore, replace the thin links U in the fermion action with $\hat{U}$.

While the backprojection (Eqs. (59), (60)) produces an element of the gauge group, it is, however, not differentiable. This turns out to be an obstacle for dynamical fermion algorithms as they require the derivative of the fermionic action with respect to the original gauge field U. Morningstar and Peardon have suggested a modification of the APE smearing procedure [96] that is both differentiable and equivalent to APE smearing for small smearing parameters α. They start by constructing the antihermitian part of the plaquettes spanned by the staples

$$A_\mu(x) = \frac{\Omega_\mu(x)U_\mu^\dagger(x) - U_\mu(x)\Omega_\mu^\dagger(x)}{2} \tag{61}$$

and making it traceless

$$S_\mu(x) = A_\mu(x) - \tfrac{1}{3}\operatorname{Tr} A_\mu(x)\,. \tag{62}$$

Exponentiating the result with a smearing parameter ρ and multiplying it on the original link

$$V_\mu(x) = e^{\rho S_\mu(x)}U_\mu(x) \tag{63}$$

gives the so-called stout link $V_\mu(x)$. For small smearing parameters, stout link smearing with a smearing parameter $\rho = \alpha/2(D-1)$ is equivalent to APE smearing.

There are many variants of the smearing procedure that are commonly used. The simplest one is the repeated application of the smearing procedure. One can *e.g.* use the $V_\mu(x)$ from Eq. (63) as an input to Eq. (61) instead of the original thin link $U_\mu(x)$. If the number of steps is kept finite, the procedure still amounts to a continuum irrelevant redefinition of the fermion action.

Instead of repeating the entire smearing procedure n times, it is also possible to change the staples used and the smearing parameter upon each application. Hasenfratz and Kenchtli [97] suggested a smearing procedure along these lines consisting of $D-1$ steps. They construct an APE-smeared link out of staples that are smeared themselves. This nested smearing is a variant of the APE smearing leaving out all directions that would cause a link to be outside the adjacent elementary hypercubes of the original target link. This nesting is then repeated until thin links are used in the $(D-1)^{\text{st}}$ step. This smearing procedure is, therefore, known as hypercubic or HYP smearing. An analytic variant of this procedure, the hypercubic exponential (HEX) smearing [38] is also in use today.

To illustrate the effect that smearing has on the eigenmode spectrum of the Wilson operator, Fig. 8 is plotting the entire spectrum of massless Wilson operators on a single gauge configuration of topological charge 1. Remember that the physically relevant low momentum modes are in the vicinity of the origin and that for the free case and for Ginsparg–Wilson, and staggered fermions the physical eigenmodes spread from the origin along the imaginary axis resp. a circle touching it (*cf.* Fig. 5). For the interacting case, we see that the eigenmodes of the Wilson operator do not touch the imaginary axis at all indicating a large additive mass renormalization. In addition, the would-be chiral mode on the real axis is far away from the low lying complex modes indicating a large mixing with doubler modes.

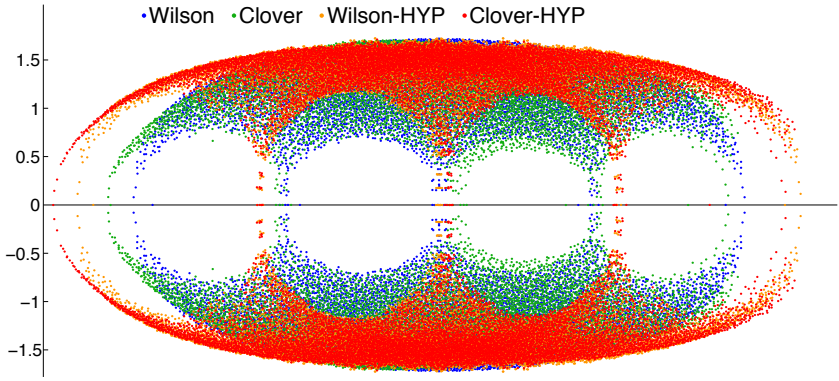

Fig. 8. Eigenvalue spectrum of Wilson-type operators on one single gauge field background on a 6^4 lattice. Data by courtesy of Dürr [98, 99].

Adding a clover term (Eq. (36)) with the tree-level $c_{\mathrm{SW}} = 1$ does mitigate both these effects somewhat as does one step of HYP-smearing. The combined effect of clover improvement and smearing, however, does result in a significantly improved operator spectrum in the relevant region.

Similarly, beneficial effects of smearing can be observed for staggered fermions. In their case, a gluon field with a momentum component $\sim \pi/a$ near the cutoff can transform between the staggered "tastes". A suppression of these spurious interactions that are absent in the continuum, therefore, improves the degeneracy between the physical and remaining doubler branches and leads to a smaller breaking of the taste symmetry.

One might be worried about the effect of iterated smearing on the locality of the fermion operator. In fact, the locality of the fermion operator itself is not affected by the smearing at all. Changing the link variables in the fermion operator does not alter the sites connected to each other via these links. What is affected by link smearing is the fermion to gauge field coupling: it acquires a momentum dependent form factor. For small α, per-

turbation theory tells us that the gauge field coupling is smeared out after N steps over an effective radius squared of [100]

$$\langle r^2 \rangle_{\text{eff}} = \frac{a^2 N \alpha}{D-1} \,. \tag{64}$$

For fixed α and N, therefore, the coupling should be local in the continuum limit. This assertion has been tested numerically for the case of 6-step stout smearing [101]. As one can see in Fig. 9, the sensitivity of the fermion operator towards a variation of the gauge field is bounded from above by an exponential in lattice units. On top of that, the coupling is still ultralocal. It is exactly 0 outside of the smearing radius.

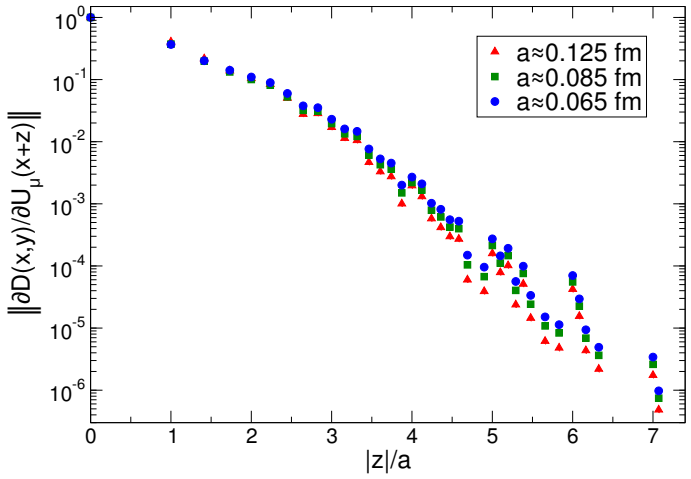

Fig. 9. Locality of the gauge field to fermion coupling for a 6-step stout smeared action. As one can clearly see, the exponential decay of the coupling with distance in lattice units has an envelope that is independent of lattice spacing. Results and figure from [101].

3. Computing the path integral

3.1. Fermion fields and observables

Until now, we have discussed how to discretize both gauge field and fermion actions on a lattice. As a next step, we would like to compute the expectation values of fermionic and gauge field observables. For the gauge fields, this seems straightforward, but the classical limit of fermions are anticommuting Grassmann fields. Assuming that we have a single staggered fermion field (with one component per lattice site) on a lattice with N points,

the implementation of the full Grassmann algebra would require an object with 2^N components. As $N \sim 10^6$ for a 32^4 lattice, which is not large by today standards, this is absolutely prohibitive.

In order to proceed, we note that, in general, the fermion action is bilinear in the fermion fields

$$S_F = \bar{\psi} D \psi \,. \tag{65}$$

Denoting the gauge action by S_G, the partition function Eq. (8) takes the form

$$\mathcal{Z} = \int \prod_{x,\mu} [dU_\mu(x)][d\bar{\psi}(x)][d\psi(x)] e^{-S_G - \bar{\psi} D \psi} \,. \tag{66}$$

Using the rules of Gassman integration, we can formally integrate out the $\bar{\psi}$ and ψ fields in Eq. (66) to obtain

$$\mathcal{Z} = \int \prod_{x,\mu} [dU_\mu(x)] \det D[U] e^{-S_G} \,. \tag{67}$$

In order to obtain expectation values of observables, we also need to integrate out the fermion fields in the numerator of Eq. (6). For gluonic observables, this is straightforward. For fermionic observables, we take as an example the generic fermion bilinear $\psi_\alpha(x)\bar{\psi}_\beta(y)$, where α and β generically denote all spinor and flavour indices. We obtain

$$\begin{aligned} &\int \prod_{x,\mu} [dU_\mu(x)][d\bar{\psi}(x)][d\psi(x)] \psi_\alpha(x)\bar{\psi}_\beta(y) e^{-S_G - \bar{\psi} D \psi} \\ &= \int \prod_{x,\mu} [dU_\mu(x)] \det D[U] D^{-1}_{\alpha,\beta}(x,y) e^{-S_G} \end{aligned} \tag{68}$$

so, here too, the path integral over the fermionic fields may be replaced by a simple factor $\det D[U]$ in the gluonic path integral or, said differently, by adding an effective gluonic action of the form $-\ln \det D[U]$ to S_G. We now introduce the shorthand notation

$$\langle O[U] \rangle := \frac{1}{\mathcal{Z}} \int \prod_{x,\mu} [dU_\mu(x)] O[U] e^{-(S_G - \ln \det D[U])} \,. \tag{69}$$

For more complex fermionic observables, one can show that the Wick theorem is reobtained with the contractions given by the corresponding inverse of the fermion matrix. We can *e.g.* obtain

$$\langle 0 | T \left(\left(\bar{\psi}_u \gamma_5 \psi_d\right)_x \left(\bar{\psi}_d \gamma_5 \psi_u\right)_y \right) | 0 \rangle = \left\langle \mathrm{Tr} \left(D_u^{-1}(x,y) \gamma_5 D_d^{-1}(y,x) \gamma_5 \right) \right\rangle \tag{70}$$

which, by using γ_5-hermiticity (Eq. (35)), can be rewritten into

$$\langle 0|T\left(\left(\bar{\psi}_u\gamma_5\psi_d\right)_x\left(\bar{\psi}_d\gamma_5\psi_u\right)_y\right)|0\rangle = \left\langle \mathrm{Tr}\left(D_u^{-1}(x,y)D_d^{-1^\dagger}(x,y)\right)\right\rangle , \quad (71)$$

where u and d denote the quark flavours and the trace is taken over colour and spin indices. The observable Eq. (70) can be diagrammatically represented as shown in the left-hand panel of Fig. 10.

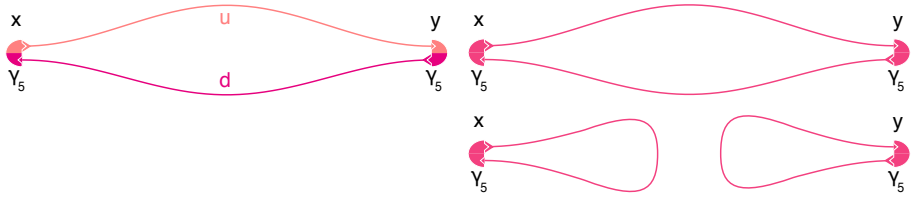

Fig. 10. Diagrammatic representation of the Wick contraction of a flavour non-singlet propagator (left) and the two contractions of a flavour singlet propagator (right).

Similarly, for a flavour-singlet observable, we obtain

$$\langle 0|T\left(\left(\bar{\psi}\gamma_5\psi\right)_x\left(\bar{\psi}\gamma_5\psi\right)_y\right)|0\rangle = \left\langle \mathrm{Tr}\left(D^{-1}(x,y)\gamma_5 D^{-1}(y,x)\gamma_5\right)\right\rangle + \left\langle \mathrm{Tr}\left(D^{-1}(x,x)\gamma_5\right)\mathrm{Tr}\left(D^{-1}(y,y)\gamma_5\right)\right\rangle \quad (72)$$

which has a disconnected contribution with a double trace in addition to the single-trace connected contribution. The diagrammatic representation is shown in the right-hand panel of Fig. 10.

3.2. Stochastic evaluation of the path integral

Having set up the framework of lattice QCD, we can now proceed to stochastically evaluate the path integral Eq. (69), computing expectation values of target observables. It is clear from Eq. (69) that the expectation value of the target observable O is just a weighted average over the observable computed on all possible gauge field backgrounds $O[U]$ with a weight $\exp(-S_U)$ and the effective action $S_U = S_G - \ln\det D[U]$. The most straightforward stochastic evaluation of the path integral would, therefore, consist of producing random gauge configurations, computing the effective action S_U on them and taking the weighted average. This procedure is very inefficient though because most of the configurations will be exponentially suppressed.

A more promising approach is known as importance sampling. Instead of generating the gauge fields with a uniform random weight, we can produce them with a weight $\propto \exp(-S_U)$. It is important to note that this is

only possible if S_U is real which, in turn, requires the fermion determinant $\det D[U]$ to be real and positive. We have seen in Sect. 2.3 that γ_5-hermiticity implies a real fermion determinant. In addition, the eigenmodes of all massless fermion operators we have covered possess a nonnegative real part and consequently $\det D[U]$ is positive definite for any positive bare mass. For all fermions retaining a remnant of chiral symmetry, *i.e.* naive, staggered and Ginsparg–Wilson fermions, there is no further subtlety. For fermions that explicitly break chiral symmetry however, like Wilson-type fermions do, an additive mass renormalization is required that typically renders the bare mass negative. The positivity of the fermion determinant has then to be ensured *a posteriori* and we will discuss in Sect. 3.4 how to check this important property in the numerical treatment.

Assuming that we may use an importance sampling technique, we label the gauge fields obtained with a weight $\propto \exp(-S_U)$ as U_i. The expectation value of an observable is then given by a straight, unweighted average

$$\langle O \rangle = \lim_{N\to\infty} \frac{1}{N} \sum_{i=1}^{N} O[U_i] \,. \tag{73}$$

Truncating the sum after a finite number of gauge configurations, we obtain an estimate of the observable

$$\hat{O} = \frac{1}{N} \sum_{i=1}^{N} O[U_i] = \langle O \rangle + \mathcal{O}\left(\frac{1}{\sqrt{N}}\right) \tag{74}$$

which is affected by a standard statistical error of the order of $1/\sqrt{N}$. Interpreting $\exp(-S_U)$ as a Boltzmann weight, the importance sampling technique might also be viewed as generating microstates of a thermodynamic system with the correct equilibrium distribution.

Except for simple cases of noninteracting theories however, it is usually not straightforward to generate gauge configurations with a weight proportional to $\propto \exp(-S_U)$. Typically, update algorithms are used that generate a gauge configuration based on a previous one using a stochastic technique. The simplest of these, the Metropolis algorithm [102], proceeds in several steps. Starting with an initial gauge configuration U_0, one iterates through the following steps:

1. Generate U_k from U_{k-1} by a small random change.
2. Measure the change in the action $\Delta S = S_U[U_k] - S_U[U_{k-1}]$.
3. Accept the change if $\Delta S \leq 0$.
4. Accept the change with a probability $e^{-\Delta S}$ if $\Delta S > 0$.

The resulting Markov chain of gauge configurations U_i will asymptotically (for large i) contain gauge configurations with the correct weight distribution[3]. There are some caveats, however, that need to be realized. First, consecutive gauge configurations are not independent. The "time"-series U_i will, therefore, have some autocorrelation, which has to be taken into account. As a consequence, the system will also not reach thermal equilibrium instantly and a number of initial configurations will have to be discarded because they suffer from thermalization effects. Finally, one not only needs to make sure that the configurations produced have the correct relative weight, but also that any possible configuration can be reached by the algorithm with a finite probability. This property is known as ergodicity. In practice, some critical observables are typically monitored to ensure the system has sensible autocorrelation times, is thermalized and ergodic. We will come back to this point in Sect. 3.4.

The algorithm most widely used today for evaluating the partition function of lattice QCD is the hybrid Monte-Carlo (HMC) algorithm [103–110]. It is an essential extension of the Metropolis algorithm that replaces the small random change of the first step, which is very inefficient in full QCD, by a more global modification of the gauge field. This global modification proceeds through first reinterpreting the fermion determinant $\det D[U]$ as the contribution to the partition function of an auxiliary scalar pseudofermion field Φ via [111]

$$\det D[U] = \int \prod_x [d\Phi^\dagger(x)]\,[d\Phi(x)]\, e^{-\Phi^\dagger \left(D^\dagger[U]D[U]\right)^{-1/2}\Phi} \tag{75}$$

and then evolving the resulting system classically in a fictitious time with a Hamiltonian

$$\mathcal{H} = \tfrac{1}{2}\Pi^2 + S\,, \qquad S = S_G + \Phi^\dagger \left(D^\dagger[U]D[U]\right)^{-1/2}\Phi\,, \tag{76}$$

where Π are randomly initialized conjugate momenta. This procedure guarantees that as long as the classical evolution part was carried out with sufficient accuracy, the change in the action ΔS will be moderate despite the global nature of the change in the gauge field. It will also provide the value of ΔS, which might otherwise require substantial effort to determine. For further details on the HMC algorithm, the reader is referred to the introductory literature [5–9, 11, 12].

In more general terms however, it should be clear at this point that independent of the specifics of the update algorithm, the numerically difficult part of lattice QCD, are the fermion fields. The change in the gauge action

[3] For more details and a proof of this statement, see *e.g.* [12].

upon modification of a single link *e.g.* is easy to compute. One only needs to compute the adjacent plaquettes *i.e.* take some products and traces of 3×3 matrices. Even the gauge action of the entire system can be computed by $\mathcal{O}(N)$ such operations, where N is the number of lattice points. Typical values of N used today range from $N \sim 10^6$ for a 32^4 lattice to $N \sim 10^8$ for a 96^4 lattice, which results in a manageable computational effort.

For the fermion fields, on the other hand, one needs to compute determinants or functions like inverse square roots (see Eq. (75)) of matrices that in the case of staggered fermions are $3N \times 3N$ and $12N \times 12N$ for other fermion formulations. It is not possible to significantly reduce the number of lattice points N either. Lattices have to be large enough in size to accommodate the relevant physics — typically at least a few fm in each direction. They have to be fine enough, on the other hand, that the lattice spacing itself is firmly within the perturbative regime so that the nonperturbative physics is reliably captured. Additionally, carrying out the continuum limit requires having a range of lattice spacings. Typically, they are chosen to be in a range of $a \sim 0.05$–0.1 fm.

As a result, the computational cost of generating lattice QCD ensembles arises almost entirely from the fermions. It has, therefore, been customary in the early days of lattice QCD to eliminate this cost entirely by a mean field approximation. This can be achieved by simply ignoring the fermion determinant $\det D[U]$ in the path integral Eq. (68). In the lattice literature, this is referred to as the quenched approximation. Although it has worked surprisingly well in some cases, it has been largely phased out nowadays due to its uncontrolled nature.

3.3. Staggered rooting

For staggered fermions, the numerical evaluation of the path integral poses one additional problem. Since doubler fermions were not entirely eliminated but merely the fermion multiplicity reduced to $2^{D/2}$ or 4 in 4 dimensions, the effective action term $-\ln\det D[U]$ describes four fermion species instead of one. Very early on, it was suggested by Marinari, Parisi and Rebbi [112] that one could just divide this effective action by $2^{D/2}$, which corresponds to taking the $2^{D/2^{\text{th}}}$ root of the fermion determinant. Whether this is a valid procedure has been widely discussed in the literature since. For the free case, Adams [43] has proven that the procedure is valid for any $m > 0$. He could show that the free staggered operator can be decomposed into 4 single flavour operators that have an identical spectrum.

In the interacting case, it is instructive to again look at the eigenmode spectrum of the Dirac operator. In Fig. 11, the physically relevant part of the eigenmode spectrum of the staggered operator is plotted on a single

gauge configuration and for different smearing levels. As a comparison, the corresponding eigenmodes of the fully chirally symmetric overlap operators are plotted, where the field transformation Eq. (53) to continuum chirality has already been performed so that the eigenmodes lie along the imaginary axis. While at low smearing level, there seems to be no resemblance whatsoever between the spectra, one can see at high smearing levels that an approximate 4-to-1 correspondence pattern emerges between staggered and overlap eigenmodes (up to a renormalization factor). This seems to suggest that in the continuum limit, the staggered fermion determinant may indeed decompose into 4 degenerate single flavour determinants and that there are only small corrections at finite lattice spacing if one properly suppresses the coupling between the flavours. More evidence for this point of view is presented in [44, 48].

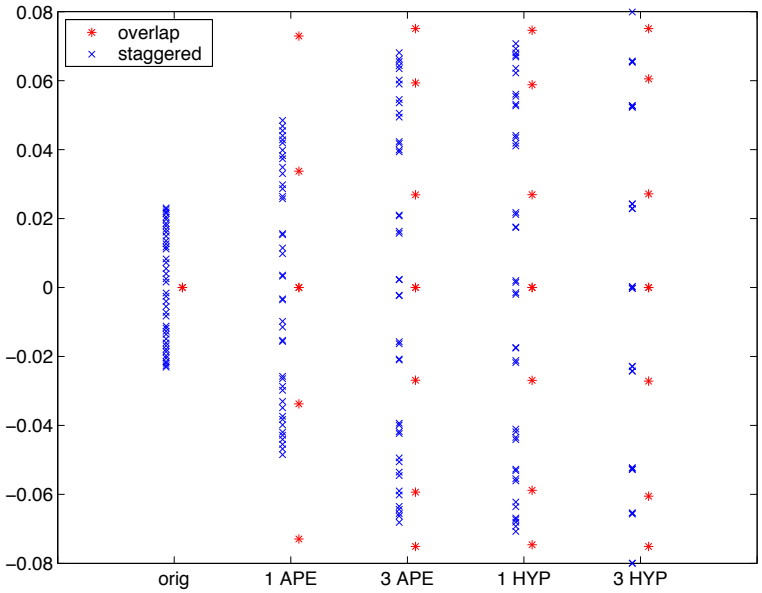

Fig. 11. Comparison of low lying eigenmodes of the staggered and overlap operators (after chiral rotation Eq. (53)) with different smearing levels on a single gauge configuration according to [48]. As one can see, after sufficient smearing the eigenmodes of the staggered operator form approximate quadruples that correspond to a single overlap eigenmode up to a renormalization factor.

There is one caveat to this argument however. While the near-degeneracy may be good, it is not exact at finite lattice spacing in the interacting theory. And since fermionic lattice observables generically involve the inverse of the fermion matrix (*cf.* Eq. 68), there is potentially a huge difference between

an approximate and a true zero mode if the mass is small. An observable that is especially sensitive to this effect, the one flavour chiral condensate in the Schwinger model, is plotted in Fig. 12. As one can clearly see, the behaviour of staggered and overlap fermions, while similar at high masses, is dramatically different at low masses. Specifically, the continuum limit at zero mass of the staggered theory is wrong. One does, however, obtain the correct $m = 0$ result with staggered fermions when the continuum limit is first taken at finite mass and the chiral limit afterwards. This subtle behaviour has to be kept in mind when dealing with staggered fermions. When one avoids this dangerous region however, there is substantial evidence that rooted staggered fermions produce correct results [45–61] although there are some dissenting opinions [62, 65].

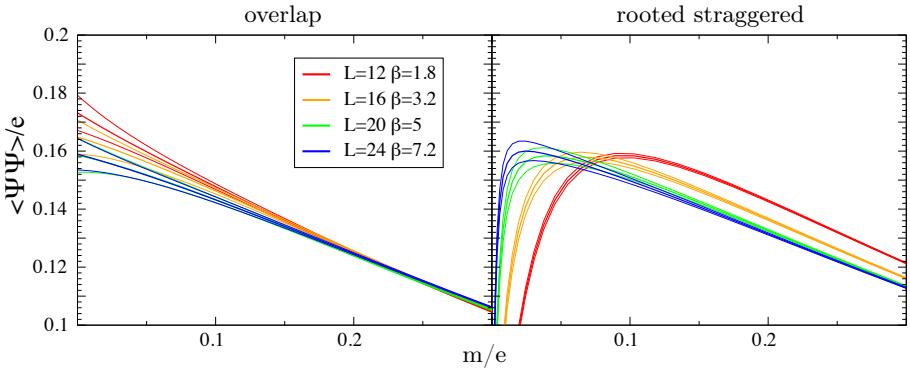

Fig. 12. Chiral condensate of the 1-flavour Schwinger model for overlap and rooted staggered fermions *versus* fermion mass for different lattice spacings from [44]. While for overlap fermions the continuum and chiral limits commute, one has to first perform the continuum limit at large enough mass for staggered fermions before going to the chiral limit.

3.4. Some important crosschecks

As already mentioned in Sect. 3.2, it is important to monitor the behaviour of the update algorithm to ensure a correct sampling of configuration space. The most straightforward technique is to monitor a simple observable such as *e.g.* the plaquette. Figure 13 shows a simple example where the initial thermalization is clearly visible.

The plaquette, however, is a rather well behaved observable that thermalizes and decorrelates relatively quickly. This property is connected with the plaquette being a very local observable and one might underestimate the true autocorrelation and thermalization time of the system by looking at it exclusively. It has, therefore, become customary to monitor other, more global observables of the system, too. One example of such an observable

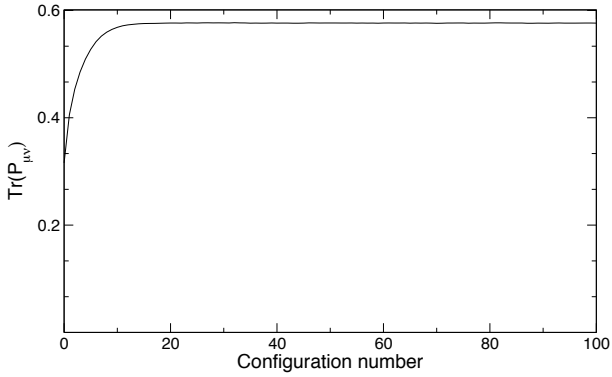

Fig. 13. Illustration of the evolution of the plaquette in simulation time.

that is in wide use today is the topological charge. It is a global property of the gauge field and the fermion operator that can only change in integer steps on typical hypertoroidal geometries. In the continuum, the topological charge is defined as

$$Q = \frac{g^2}{32\pi} \int d^4x G^*_{\mu\nu} G_{\mu\nu} \tag{77}$$

which can be easily generalized on the lattice [113]. Its relation via the index theorem [32] to the zero modes of a chiral fermion operator allows for an alternative extraction method which, however, is much more demanding computationally. An example from a recent work is displayed in Fig. 14.

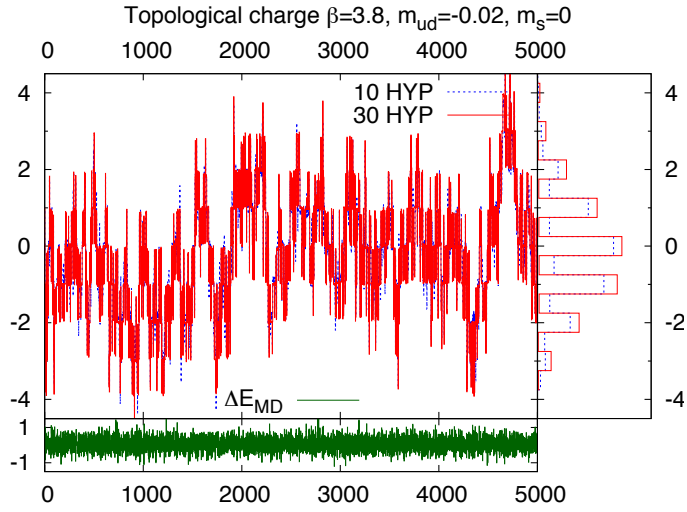

Fig. 14. History and histogram of topological charge from a recent large scale simulation [114]. The relevant autocorrelation time of $|Q|$ in this instance was determined to be 27.3 ± 7.4.

Studying the topological charge autocorrelation as one goes to the continuum limit, Schaefer, Sommer and Virotta [115] have pointed out a potentially severe problem. Their results are displayed in Fig. 15. As one can clearly see, the topological charge does not tunnel anymore at the finest lattice investigated for the entire Markov chain but, instead, remains frozen at a certain value. The details of this behaviour are, of course, dependent on the specific action and algorithm used, but there is a physical cause for it which is again maid clear by looking at the eigenmode spectrum of the fermion operator.

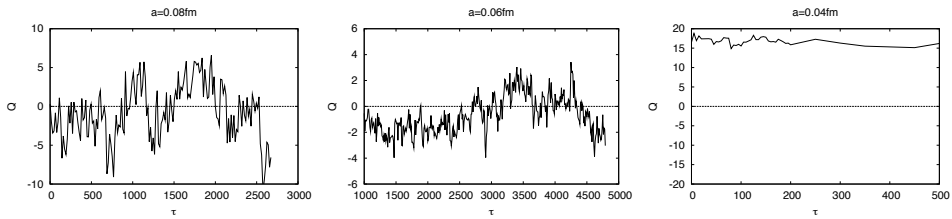

Fig. 15. History of topological charge for for different lattice spacings from [115].

Remember that for Wilson-type operators topological modes lie along the real axis. The number of modes in the physical branch determines the topological sector (*cf.* Fig. 8). To change topological sector, these modes therefore need to either appear or disappear. The only possibility for this to happen is, however, that either a pair of complex conjugate modes approaches the real axis, mix and split into a physical, and doubler chiral mode or the other way round. As one approaches the continuum however, this is not easily possible in a continuous manner. Chiral symmetry is restored and there is a gap developing between the physical and the doubler branches. The fermion operator will, therefore, have to develop a discontinuity in the underlying gauge field at the boundary of a topological sector.

This behaviour should, therefore, be more pronounced the better the fermions discretization realizes chiral symmetry. In fact, it has been observed earlier that for Ginsparg–Wilson fermions changing the topology is a far greater challenge already on relatively coarse lattices [116–118].

Several suggestions have been made over the years on how to deal with this problem. For Ginsparg–Wilson fermions, special update algorithms have been proposed [119]. An alternative point of view is that fixing a topological sector is only a finite volume effect that can be corrected for [120]. Ultimately, for large enough volumes, subvolumes will decorrelate and reproduce the correct fluctuation pattern even if the overall topological charge is fixed. Along similar lines, it was suggested to use open boundary conditions [121] for which topological charge is not an integer. Here too, the open boundary results in additional finite volume effects that can ultimately be

eliminated by a proper infinite volume limit. For current lattice calculations however, the potentially long autocorrelation times in the continuum limit are not a limiting factor yet. For fermion discretizations that do not have exact chiral symmetry, these effects become relevant only for lattices finer than $a \sim 0.05$ fm.

For Wilson-type fermions, one needs to perform another crucial check. Because of the additive mass renormalization, the fermion determinant was not guaranteed to be positive definite. In terms of the eigenmode spectrum, a negative fermion determinant can only appear when an odd number of real modes is negative after the additive mass renormalization has been applied (*cf.* Fig. 8). In principle, one should therefore monitor the real modes of the fermion operator. Since this is computationally expensive, another quantity is typically monitored that is closely related but also directly obtainable from the simulation itself. Remember that in every update step, a fermion matrix has to be inverted (on a source vector) in order to construct the pseudofermion action Eq. (75). This inversion is performed iteratively and the number of iterations is very sensitive to the condition number of the matrix, *i.e.*, the ratio of its largest to smallest eigenvalue. If during the classical evolution in the pseudo-time a real mode would come close to the origin, it would immediately be recognizable as an increase in the iteration count of the inverter. In the limiting case of a zero mode, the inverter would

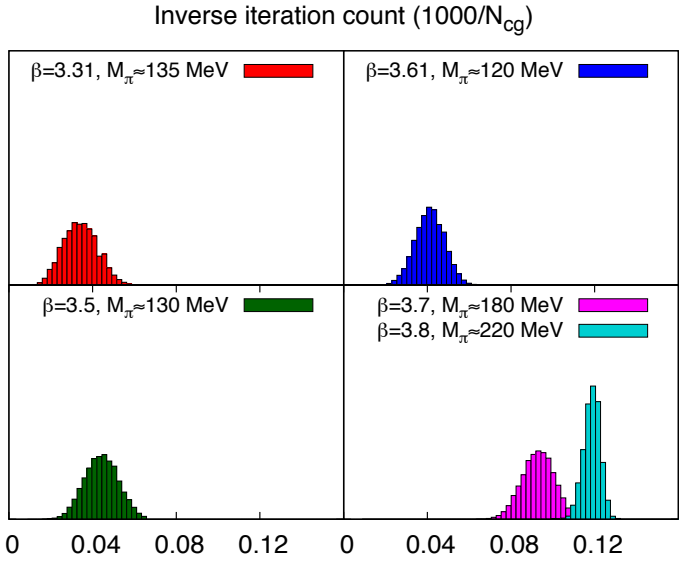

Fig. 16. Histogram of the inverse iteration count in the inversion of the fermion operator from a recent large scale simulation [114].

not converge and the corresponding gauge configuration is called exceptional. One can, therefore, plot the iteration count or, as in Fig. 16, the histogram of the inverse iteration count. If the tail of the distribution has a safe distance from 0, one can conclude that no real mode has crossed over to the negative side and, therefore, the fermion determinant is indeed positive.

Some further checks of algorithm stability and efficiency that are routinely done include monitoring the acceptance rate and the forces in the classical evolution of the fermion field. Sometimes hystereses are recorded with respect to varying fermion masses or the gauge coupling when one suspects the proximity of an unphysical phase transition due to lattice artefacts. In general, one can say that lattice QCD has a large set of tools for checking the integrity of the simulation algorithms.

4. An example calculation: hadron masses

4.1. Skeleton of a lattice calculation

With the basic techniques established, the next step is to actually make physical predictions using lattice QCD. We will look at the computation of ground state light hadron masses [101, 122] as a prototypical example. In principle, the strategy is straightforward: we want to go to the physical point and read off the target observables. But the physical point can, of course, never be reached directly. One always has to extrapolate to the continuum limit and to infinite volume. In addition, the physical values of the parameters of the lattice QCD action, namely the gauge coupling and the quark masses, are unknown. Hence it is necessary to define the physical point through a set of quantities that can be measured both experimentally and on the lattice and to interpolate or extrapolate lattice results to the physical point thus defined.

Typical lattice QCD calculations currently include two flavours of degenerate light quarks, a strange quark and possibly a charm quark. In lattice terminology, these setups are referred to as $2+1$ resp. $2+1+1$. Isospin splitting is usually treated as a perturbation while the effects of b and t quarks can, generally, be ignored at the current level of precision. In such a setup, each lattice calculation has 3 or 4 parameters: the gauge coupling g and the masses of the quarks m_{ud}, m_s, and possibly m_c. Through dimensional transmutation, the gauge coupling is closely linked to the scale of the theory, *i.e.* the lattice spacing. Light and strange quark masses, on the other hand, are related to the masses of the pseudoscalar mesons. To leading order, this relation reads [123]

$$M_\pi^2 \propto 2m_{ud}\,, \qquad M_K^2 \propto m_s + m_{ud}\,. \tag{78}$$

One can, therefore, characterise an ensemble of gauge configurations by lattice spacing and the observable quantities M_π and $\sqrt{2M_K^2 - M_\pi^2}$ instead of g, m_{ud} and m_s. In addition, the size of the lattice is a relevant parameter.

Figure 17 displays these simulation parameters for some recent lattice QCD calculations. Since it is substantially less demanding numerically, a lot of calculations are still performed at large pion masses, relatively coarse lattice spacings and small volumes. One can, however, reach physical pion masses today at multiple lattice spacings and volumes as large as $(6\ \mathrm{fm})^3$, which allows a controlled continuum and infinite volume extrapolation as well as an interpolation to physical M_π to be performed.

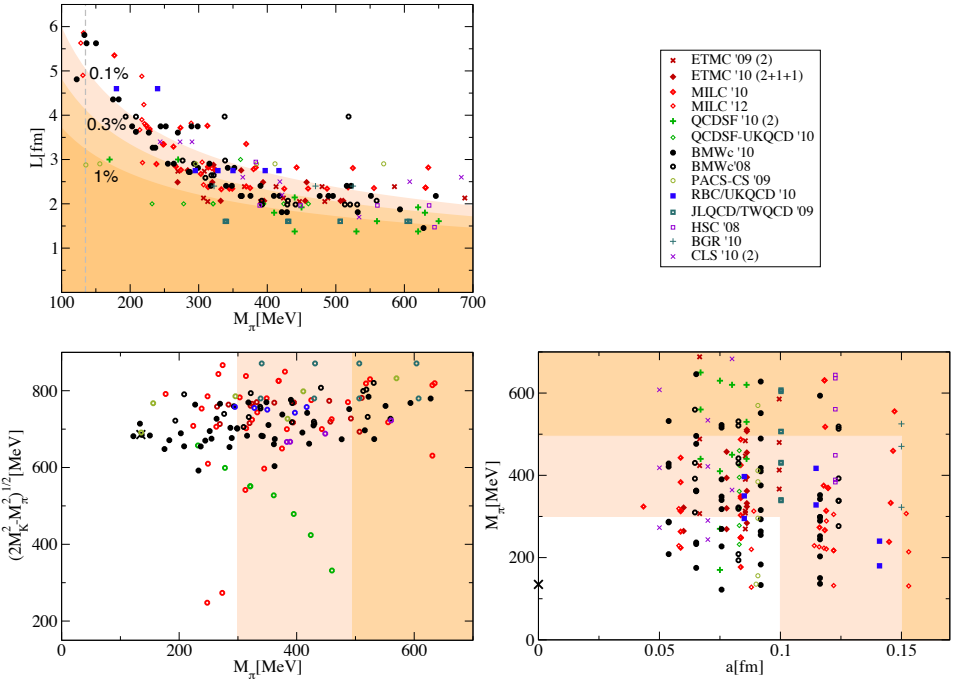

Fig. 17. Plot of simulation parameters of some recent lattice calculations with dynamical fermions following [124]. Data are from ETMC'09(2) [125], ETMC'10 (2+1+1) [126], MILC'10 [55], QCDSF'10(2) [127], QCDSF-UKQCD'10 [128], BMWc'08 [101], BMWc'10 [114], PACS-CS'09 [129, 130], RBC-UKQCD'10 [131, 132], JLQCD/TWQCD'09 [133], HSC'10 [134], BGR'10(2) [135] and CLS'10(2) [136]. The cross in the lower left- and right-hand plots denote the physical point. The percent marks in the upper left-hand plot indicate the estimated relative finite volume corrections on the pion mass according to [137].

4.2. Extraction of hadron masses

As a first step towards a physical prediction, we need to actually measure the hadron masses on our ensembles of gauge configurations. We first choose two (not necessarily different) operators $O_{1/2}$ that couple to the target hadron $|h\rangle$

$$\langle h|O_{1/2}|0\rangle \neq 0\,. \tag{79}$$

We then compute the correlator

$$G(t,0) = \langle 0|O_2^\dagger(t)O_1(0)|0\rangle = \langle 0|e^{\mathcal{H}t}O_2^\dagger e^{-\mathcal{H}t}O_1|0\rangle \tag{80}$$

as described in Sect. 3.1. Inserting a complete set of eigenstates

$$\mathbb{1} = \sum_n \frac{1}{2E_n}|n\rangle\langle n|\,, \qquad \mathcal{H}|n\rangle = E_n|n\rangle\,, \quad E_0 = 0 \tag{81}$$

in the standard fashion, we obtain

$$G(t,0) = \sum_n \frac{\langle 0|O_2^\dagger|n\rangle\langle n|O_1|0\rangle}{2E_n} e^{-E_n t}\,. \tag{82}$$

If our target state $|h\rangle$ happens to be the ground state, we can extract its mass $M = E_h$ by simply going to asymptotic times

$$G(t,0) \overset{t\to\infty}{\longrightarrow} \frac{\langle 0|O_2^\dagger|h\rangle\langle h|O_1|0\rangle}{2M} e^{-Mt} \tag{83}$$

and measuring the exponent in the decay of the propagator with time separation. One can also define an effective mass

$$M_{\text{eff}} = \ln \frac{G(t,0)}{G(t+1,0)} \overset{t\to\infty}{\longrightarrow} M \tag{84}$$

that will signal when the regime has been reached where excited state contributions are negligible.

On a lattice of finite time extent T, it is, of course, not possible to go to asymptotic times. In fact, due to the periodicity of the lattice in time direction, the propagator $G(t,0)$ will typically be dominated by backward propagating states for $t > T/2$. In fact, for $T \gg T - t$, we can find

$$G(t,0) \overset{T-t\to\infty}{\longrightarrow} \frac{\langle 0|O_1^\dagger|\tilde{h}\rangle\langle \tilde{h}|O_2|0\rangle}{2E_{\tilde{h}}} e^{-E_{\tilde{h}}(T-t)}\,, \tag{85}$$

where $\tilde{h}$ is the lowest energy state coupling to the adjoint of the source operators

$$\langle \tilde{h}|O_{1/2}^\dagger|0\rangle \neq 0\,. \tag{86}$$

In principle, there are also contributions to the propagator from multiple windings around the time direction. Each additional winding in forward direction *e.g.* gives an additional factor e^{-MT}, which, however, only gives a tiny correction to the prefactor and is, therefore, irrelevant for extracting masses.

As a typical example, the charged pion mass can be extracted using a source operator

$$O_1 = \left(\bar{\psi}_u \gamma_5 \psi_d\right)_{\vec{x}} . \tag{87}$$

Using a sink operator O_2 of the same form, we obtain the observable discussed in Eq. (71), u and d D_u and D_d for the source point $(0, \vec{x})$ only. One can see from Eq. (71) that no additional inversions are required to go to an arbitrary sink point. In fact, we can sum over all sink points in a given time slice and thus project the final state to $\vec{p} = 0$ without any substantial additional cost. It is, therefore, customary to use as a sink operator

$$O_2 = \sum_{\vec{y}} \left(\bar{\psi}_u \gamma_5 \psi_d\right)_{\vec{y}} . \tag{88}$$

There is a wealth of additional techniques to construct efficient operators which is beyond the scope of these notes to cover and I refer the interested reader to the introductory literature for further details [9, 11, 12].

For our specific example, we have $|\tilde{h}\rangle = |h\rangle$ and also $\langle 0|O_1^\dagger|\tilde{h}\rangle\langle\tilde{h}|O_2|0\rangle = \langle 0|O_2^\dagger|h\rangle\langle h|O_1|0\rangle$ so that the prefactors as well as the masses are the same in the forward (Eq. (83)) and backward (Eq. (85)) contributions. In a region where excited state contributions are irrelevant, we therefore obtain

$$G(t,0) \propto e^{-Mt} + e^{-M(T-t)} \propto \cosh M(T/2 - t) . \tag{89}$$

We can use Eq. (89) as a fit ansatz to extract M from $G(t,0)$ or solve it with respect to M for two time slices to obtain an effective mass.

Figure 18 gives an example of an effective mass plot and corresponding fit ranges for several hadronic channels. As one can see, it is not entirely clear what is an optimal fit range to choose. It is, therefore, essential to perform fully correlated fits and monitor the fit quality. It is also good practice to perform the analysis with multiple fit ranges that seem sensible and let the corresponding spread of the results enter the systematic error.

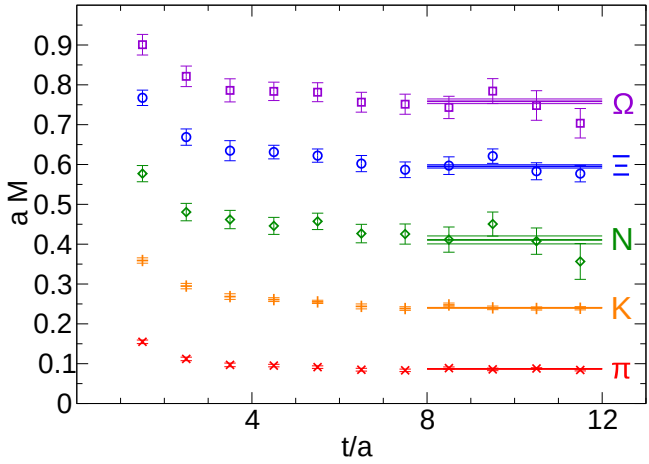

Fig. 18. Plateaus of the effective mass and fit ranges for some hadron channels from [101].

A further check for a sensible fit range is possible over a set of ensembles. If there is no excited state contribution, the fit quality Q is expected to be randomly fluctuating between 0 and 1. One can plot the CDF of the fit quality and check with a Kolmogorov–Smirnov test whether it is compatible with the expected linear rise (see Fig. 19).

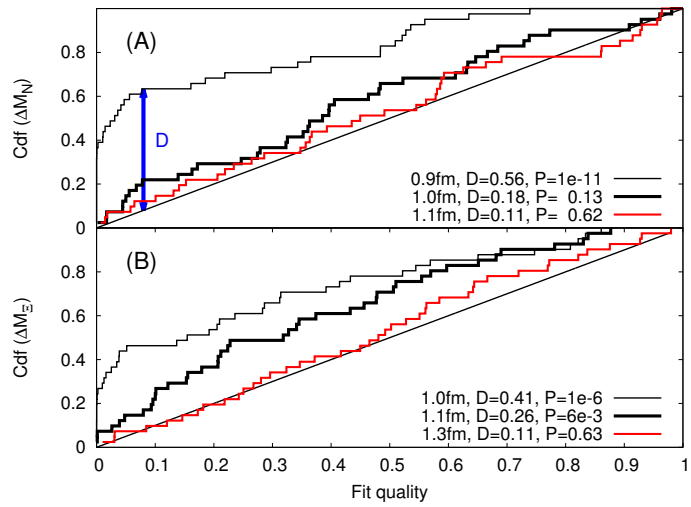

Fig. 19. Cumulative histogram of fit quality over 48 ensembles for different initial times and two observables from [122]. For each case, the legend gives the maximum distance D between expected and measured CDF as well as the probability p that they are identical according to the Kolmogorov–Smirnov test.

Extracting excited state masses from Eq. (82) is much more difficult as the contribution of excited states decays exponentially with separation. It is, in principle, possible to make an ansatz

$$G(t,0) = a_0 e^{-M_0 t} + a_1 e^{-M_1 t} \tag{90}$$

and fit for the ground state mass M_0, the excited state mass M_1 and the two prefactors a_0 and a_1. In practice, however, these fits tend to be unstable and have a limited accuracy. It is preferable in these cases to use a larger operator basis O_i and measure the full cross-correlator between its elements [138, 139]

$$G_{ij}(t,0) = \langle 0|O_i^\dagger(t)O_j(0)|0\rangle\,. \tag{91}$$

From two time slices an effective mass matrix

$$M(t,t_0) = G(t,0)G^{-1}(t_0,0) \tag{92}$$

can now be computed and its eigenvalues will asymptotically give the energies of the lowest lying states

$$\lambda_n \to e^{-E_n(t-t_0)}\,. \tag{93}$$

This so-called variational method may, in fact, be advantageous for extracting ground state masses. The reason is that after diagonalization the contamination of the ground state from the $N-1$ lowest excited states has been removed, where N is the size of the operator basis.

For the variational method to work, it is essential that each of the target states has good overlap with at least one operator of the basis. This is a nontrivial requirement and the classical example is the scalar operator

$$O_\mathrm{s} = \left(\bar\psi_u\psi_u\right)\,. \tag{94}$$

Although O_s should, in principle, couple to two-pion states, this coupling is practically zero. In order to be sensitive to two-pion states, four fermion operators like

$$O_4 = \left(\bar\psi_u\gamma_5\psi_d\right)\left(\bar\psi_d\gamma_5\psi_u\right) \tag{95}$$

need to be considered, too.

When extracting excited states, one also needs to keep in mind that the relation between discrete energy levels extracted on a finite volume lattice and the spectral density characterising an infinite volume resonance is not straightforward. If one aims at predicting the mass of a physical resonance, it is not sufficient to simply measure a corresponding energy level on the lattice. We will briefly return to this point in Sect. 4.4.

4.3. Scale setting

Being able to compute hadron masses, we can now determine the parameters of our lattice ensembles in terms of physical quantities. As outlined in Sect. 4.1, we can use the pseudoscalar meson masses M_π and M_K to locate the physical light and strange quark masses. The coupling g is related to the lattice scale and we need one additional physical observable to fix it. Setting the mass of the charm quark for cases where it is present trivially follows along the same lines and will not be further discussed.

The ideal scale setting observable should satisfy a few obvious criteria. Most importantly, it should be known from experiment with a high accuracy and it should be computable on the lattice with high precision, too. In addition, it should not depend on quark masses strongly. The most obvious choices are the masses of some heavy hadrons. In the early days of lattice QCD, the mass of the ρ meson was often used. This, however, is not an ideal choice, as the ρ is a broad resonance which makes its mass difficult to determine precisely both for the experiment and on the lattice.

A quantity that is widely used for scale setting today is the mass of the Ω baryon and to a lesser extent the cascade Ξ. Both of them can be measured precisely in experiment and on the lattice, and both have little light quark mass dependence. Also in wide use today are the pseudoscalar decay constants F_π and F_K. While they can easily be determined with high precision on the lattice, one has to keep in mind that their physical value is not obtained directly from experiment.

There is also a variety of intermediate scale setting variables that are often used in lattice calculations today. They are not directly related to any experimentally observable quantity but simple to measure on the lattice. Their physical values have to be determined initially however, which is usually done by a lattice calculation using a scale setting observable that is experimentally accessible.

One group of scale setting observables that have been in use since the early days of lattice QCD is based on the static quark potential. The potential between static sources of colour charge at a distance R in direction x_i can be expressed in terms of a Wilson loop $W_{0i}^{T\times R}$ (see Sect. 2.2) with a long extent in time direction as

$$V(R) = -\lim_{T\to\infty} \frac{\ln W_{0i}^{T\times R}}{T}\,. \tag{96}$$

Historically, the large separation limit of the force or string tension

$$\sigma = \lim_{R\to\infty} \frac{dV(R)}{dR} \tag{97}$$

has been in wide use. More recently, the Sommer scale $r_{0/1}$ [140] which is related to the force at a finite distance

$$R^2 \frac{dV(R)}{dR}\bigg|_{R=r_{0/1}} = 1.65/1 \tag{98}$$

has become a standard scale setting observable.

Even more recently, scale setting observables based on the gradient flow, an infinitesimal form of the gauge field smearing procedure, have been suggested [141, 142]. For a generic field theory with fields ϕ and action S, the gradient flow of the field ϕ is defined by

$$\dot{\phi}(x) := \frac{\partial \phi(x)}{\partial t} = -\frac{\delta S[\phi, \partial_\mu \phi]}{\delta \phi(x)} \tag{99}$$

in a flow time t. Obviously, the field is driven towards the classical solution for large flow time (see also [143]). Applying this generic concept to a gauge theory with the Wilson plaquette action (Eq. (14)), one obtains an infinitesimal form of APE smearing (Eq. (57)). A scale can now be defined by integrating the flow equation to obtain the smeared gauge fields $G_{\mu\nu}(t)$ at a finite flow time t and demanding that

$$t_0^2 \langle E(t_0) \rangle = 0.3\,, \qquad E(t) = -\frac{\operatorname{Tr} G_{\mu\nu}^2(t)}{4}\,. \tag{100}$$

According to Eq. (64), the effective smearing radius at flow time t is given by $\sqrt{8t}$ and we can use t_0 to define a lattice scale. An alternative method is to use w_0 defined via

$$t \frac{d}{dt} \left(t^2 \langle E(t_0) \rangle \right)\bigg|_{t=w_0} = 0.3\,. \tag{101}$$

Both the static quark potential and the gradient flow are purely gluonic quantities, which are much easier to measure than fermionic ones. In addition, the gradient flow method does not require fitting any data and is therefore very straightforward to implement.

4.4. Finite volume effects

As a last step before we can extrapolate the lattice results to the physical point, we need to look at the effect of the finite lattice volume. The good news is that for masses of hadrons that do not decay via the strong interaction, QCD finite volume effects are typically small. The reason for this is that QCD is a theory with a mass gap. A hadron in a finite box

will be affected by mirror charge effects, *i.e.* it will interact with itself over a distance L, where L is the spatial size of the box. Due to the mass gap of QCD, this interaction will, however, be exponentially suppressed in the lightest particle mass. Therefore, one generically expects finite volume effects to be proportional to $e^{-M_\pi L}$.

Corrections to this leading order behaviour for mesons [137, 145–149] and, to a lesser extent, baryons [144, 150] have been computed. As demonstrated in Fig. 20, they describe lattice data very well. As a rule of thumb, lattices with $M_\pi L \geq 4$ generate small finite volume corrections for non-resonant particle masses where the condition can be somewhat relaxed for lower M_π.

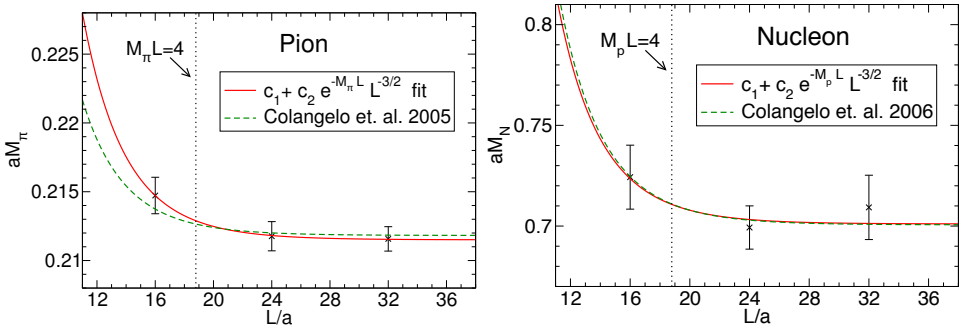

Fig. 20. Pion (left-hand panel) and nucleon (right-hand panel) mass in lattice units *versus* lattice size. Lattice data [101] agree very well with the theoretical prediction [137, 144].

For resonances, finite volume effects are more pronounced however. In the continuum, a resonance is characterized by an increase in the spectral density (see Fig. 21). In finite volume however, there are only discrete energy levels that correspond to some linear combination of the resonance and its decay products. In order to make an infinite volume prediction for the mass of the resonant states, it is, therefore, necessary to disentangle these effects.

A very simple quantum mechanical model can nicely illustrate the underlying physics. We consider a particle in a double potential well

$$V(x) = K\delta(r)\,, \qquad x \in [0, L] \quad 0 < r \ll L\,. \tag{102}$$

For an infinite separation between the two wells $K \to \infty$, the energy levels of the small left well $x < r$, representing the resonance, and the large right one $x > r$, representing the scattering states, are independent as illustrated in the left-hand panel of Fig. 22. We now introduce a coupling of the resonance by making the barrier height K finite, which causes the left- and right-hand side modes to mix (middle panel). Changing the volume of the box will then

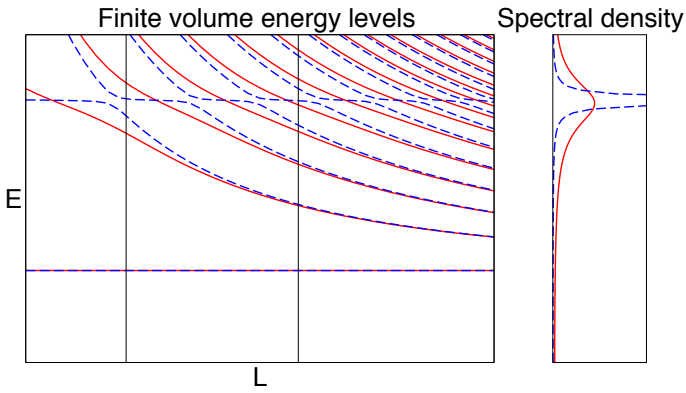

Fig. 21. Illustration of the infinite volume energy density (right-hand panel) and the corresponding finite volume energy levels (left-hand panel) plotted *versus* box size L for a narrow (dashed line) and a broad (full line) resonance. The physical ρ resonance would be much closer to the broad resonance case.

change the mixing pattern (right-hand panel) and the phenomenon of level repulsion occurs. Depending on the box size L, different modes will be in the vicinity of the uncoupled resonance energy and overlap with the wave function of the uncoupled resonance state. Measuring these energy levels for different box sizes, we can infer the energy of the uncoupled resonance and the barrier height or coupling.

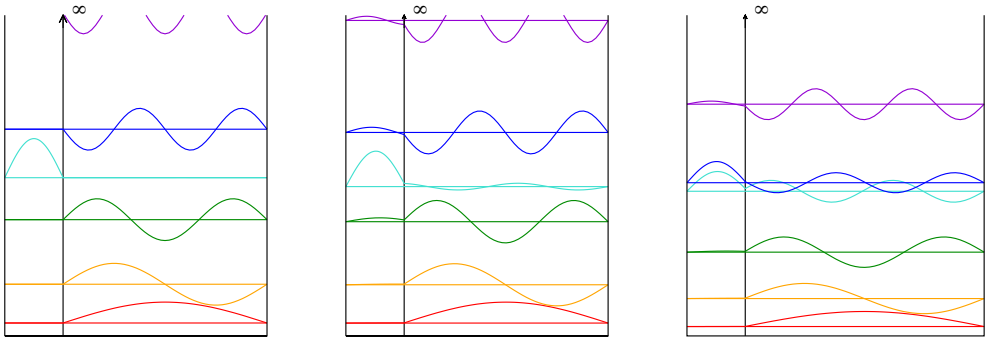

Fig. 22. Energy levels and wave functions of the double well potential model.

In a very similar manner, it is possible to treat the problem of resonances in QCD with scattering theory [101, 151–154]. The energy of the uncoupled scattering states is known — in the case of the ρ, it is simply the energy of a two pion system at the relative momenta $\vec{p}$ allowed by the volume — and one can, therefore, extract the mass and the coupling of the resonance by measuring the energy levels of the system at various finite volumes.

It should also be clear from the model consideration that not all energy levels are equally sensitive to the resonance mass. In order to have large sensitivity, the level must be close to the resonance mass itself.

4.5. Extrapolating to the physical point

We, finally, have all ingredients ready to extrapolate our target hadron mass M_X to the physical point and make a physical prediction. We have measured M_X on each ensemble and in addition M_π, M_K, and the scale setting observable M_Ξ or M_Ω. As explained in Sect. 4.1, we traded the bare parameters of our theory for M_π, M_K and $M_{\Xi/\Omega}$, so we need the correct functional dependence of M_X on these (and on the lattice size) to extrapolate to the physical point.

Generically, we can expand any heavy hadron mass M in terms of the quark masses

$$M = M^{(0)} + \hat{\alpha} m_{ud} + \hat{\beta} m_s + \dots \tag{103}$$

which, according to Eq. (78), translates into

$$M = M^{(0)} + \alpha M_\pi^2 + \beta M_K^2 + \dots \tag{104}$$

Depending on the precision of our data, we may need to add higher order terms to this expansion. The specific form of these terms depends on the expansion point we choose. For an optimal convergence radius, a Taylor expansion around finite M_π^2 and M_K^2 seems to be a good choice. Alternatively, one may perform an asymptotic expansion around $M_\pi^2 = 0$ for which chiral perturbation theory generically gives a term $\propto M_\pi^3$ as the next higher order in M_π^2 [155]. Since the lattice data are not sensitive to further terms, it is a good idea to use both ansätze

$$M = M^{(0)} + \alpha M_\pi^2 + \beta M_K^2 + \gamma \begin{cases} M_\pi^4 \\ M_\pi^3 \end{cases} \tag{105}$$

for extrapolating/interpolating to the physical point and let the spread between the results contribute towards the systematic error.

Sensible ansätze for the infinite volume behaviour have been discussed in Sect. 4.4. We can, therefore, perform a combined fit of the scale setting observable M_Ξ or M_Ω *versus* M_π, M_K and the lattice size L, introducing one fit parameter a_β for each of the bare couplings $\beta = 6/g^2$ in our ensembles. Requiring the fit to go through the physical point, which can be defined by the physical value of the ratios $M_\pi/M_{\Xi/\Omega}$ and $M_K/M_{\Xi/\Omega}$, the lattice spacings are determined.

We can then make an ansatz for the continuum limit of M_X guided by the scaling behaviour of the action (see Sect. 2). For an unimproved Wilson action, one would *e.g.* choose

$$M = M^{(0)} + \eta a + \dots , \tag{106}$$

while for a nonperturbatively improved clover action

$$M = M^{(0)} + \eta a^2 + \dots \tag{107}$$

might be more appropriate. The specific example calculation I am following used a perturbatively improved smeared clover action. Formally, its scaling is $\mathcal{O}(\alpha_s a)$, which is in between Eq. (106) and Eq. (107). Numerically, even the leading scaling term is barely relevant. It is, therefore, a very conservative choice to use both Eq. (106) and Eq. (107), and again add the spread between the results thus obtained to the systematic error.

Performing a combined continuum, infinite volume, M_π and M_K fit, we thus obtain a prediction for M_X at the physical point. An example of such a fit for the Ω and nucleon masses with the scale set by M_Ξ is displayed in Fig. 23.

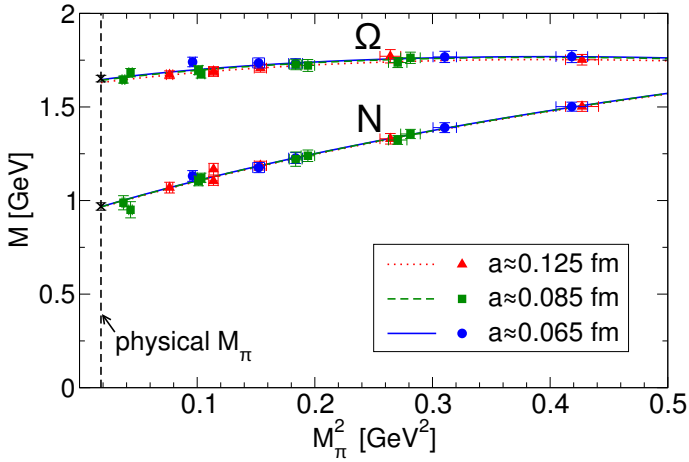

Fig. 23. Nucleon and Ω mas *versus* M_π^2 from [101]. Points represent lattice data shifted with the combined fit function to be at physical M_K^2 and corrected for finite volume effects. Curves represent the fit for 3 different lattice spacings. It is evident that the extrapolation to both the continuum limit and the physical M_π^2 is very mild.

It is interesting to note, that in the derivation of the fit function, we have so far made a choice that the lattice spacing depends only on β among the bare lattice parameters, which is known as mass independent scale setting. Since the lattice spacing is ill defined outside the physical point (*i.e.* different definitions may lead to different values), we may actually choose any other procedure as long as it coincides at the physical point. One might *e.g.* assume that outside the physical point the scale setting observable keeps the same physical value. An alternative way to Eq. (105) for parametrizing the quark mass dependence would, therefore, be

$$M = M^{(0)} + \alpha r_\pi^2 + \beta r_K^2 + \gamma \begin{cases} r_\pi^4 \\ r_\pi^3 \end{cases} , \tag{108}$$

where $r_X := M_X/M_{\Xi/\Omega}$ is the ratio of M_X to the scale setting mass. A fit with this ratio method is displayed in Fig. 24.

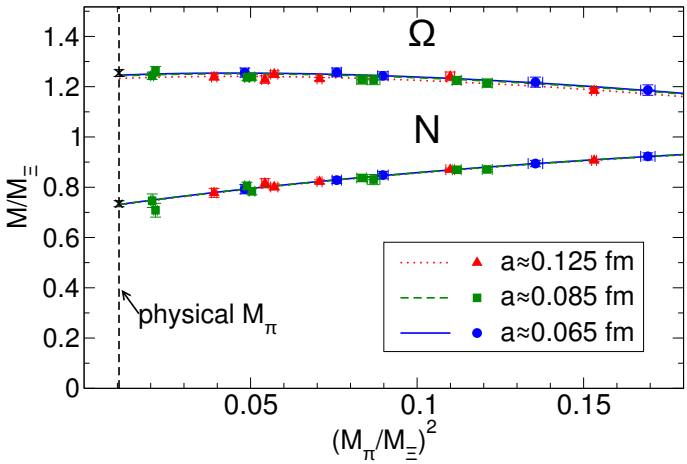

Fig. 24. Nucleon and Ω mas *versus* r_π^2 from [101]. Points represent lattice data shifted with the combined fit function to be at physical r_K^2 and corrected for finite volume effects. Curves represent the fit for 3 different lattice spacings.

4.6. Systematic errors

Having extrapolated the target observable to the physical point, we have a prediction with a statistical error. In fact, we have many predictions of the same observable — hundreds or even thousands are not uncommon. During the analysis, we had many points where a number of different procedures were reasonable — the time interval for extracting baryon masses, the scale setting observable or various fit forms — and we said that we will include the corresponding spread into the systematic error. This is what we will do now.

It is important to note that there is no uniquely correct procedure to compute the systematic error. In fact, unlike the statistical error, the systematic error cannot be computed. The systematic error tries to quantify the effects which we are not able to control — *e.g.* the size of the terms in a Taylor expansion that we truncated because our data are no more sensitive to it. It is, therefore, a guess or at best an estimate. The most important point about estimating a systematic error, therefore, is not to omit any relevant part of it. A sophisticated estimate of the error in the M_π extrapolation *e.g.* is useless if all data were obtained at a single lattice spacing or the fit window for extracting the bare masses was not varied.

Provided that we have varied our analysis procedure to cover all relevant effects, a simple procedure for estimating the systematic error would then be to take all the results and compute the spread. The average or mean of the distribution can serve as the central value. I label this procedure as flat weight.

One might be worried that with this procedure, an analysis that did not describe the data well will have the same weight as one that did. One might, therefore, put a weight to each analysis when computing the spread and the average. A reasonable weight would *e.g.* be the fit quality Q.

Another weight that is motivated by information theory is the Akaike information criterion (AIC) [156]. It estimates the information contained in a specific fit m by computing the information cross-entropy J_m of the given fit with the best one in the sample. For a large number of points, the cross-entropy is then given by

$$J_m = -\frac{\chi^2}{2} - p_m \,, \tag{109}$$

where p_m is the number of parameters of the fit and χ^2_m is given by the least square fit. The probability that a fit is correct is proportional to the exponential of the cross-entropy $\exp J_m$. The AIC punishes fits with a large number of parameters, since according to Eq. (109), χ^2 has to decrease by 2 for every new parameter to even achieve the same weight.

Although the AIC might seem to be an optimal method, it is important to note that it only gives relative weights among fits that were chosen beforehand or, in other words, that we have provided as an input a certain measure in the space of all possible fits that the AIC only modified. Since we have no *a priori* knowledge about a proper measure, even the AIC weighted systematic error is just a guess.

From a practical point of view, it is important to note, that all sensible estimates of the systematic error should give compatible values (see Fig. 25). In fact, this agreement is a valuable crosscheck for the entire analysis procedure.

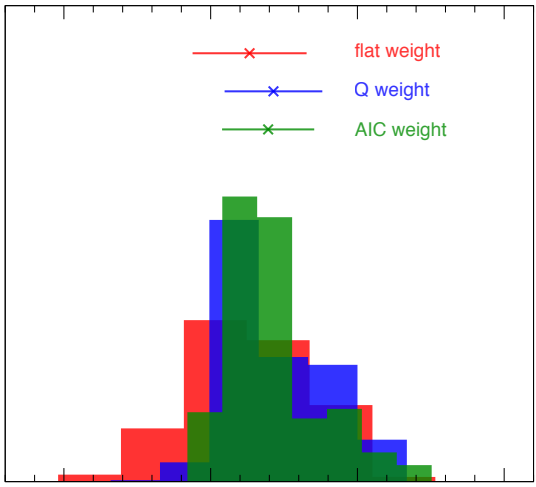

Fig. 25. Comparison of three methods to compute the systematic error.

Adding the statistical and systematic errors in quadrature, the ground state light hadron spectrum can now be computed. The result is displayed in Fig. 26.

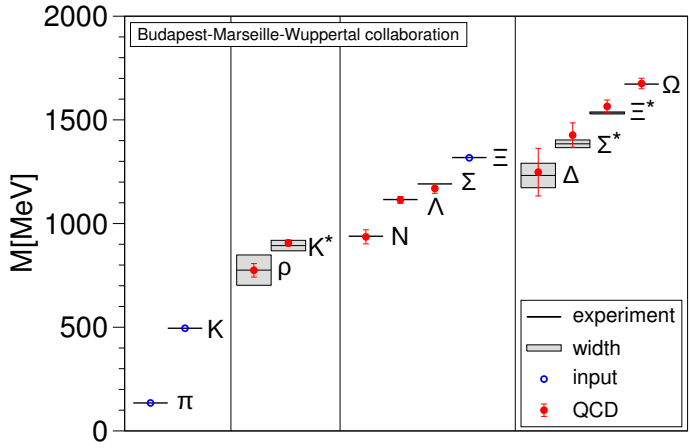

Fig. 26. The ground state light hadron spectrum from [101]. Open/blue points denote observables that were used as input quantities in the lattice calculation, while full/red points are lattice predictions with combined statistical and systematic error. Experimental values are isospin averaged and boxed denote the width of resonances.

4.7. QED and strong isospin splitting

We now turn our attention to the fine structure of the hadron spectrum. The electromagnetic and strong isospin splitting effects in the hadron spectrum are typically a few MeV. After having made physical predictions in QCD, it might seem trivial to include these effects in our lattice calculations. For the case of strong isospin splitting, this is true at least conceptually — one only needs to introduce independent u and d quark masses. From a computational point of view it is, however, extremely demanding to accommodate for the very light u quark mass. Both u and d quarks are light, but $m_u/m_d \sim 0.5$ resulting in a much worse conditioned fermion matrix. For Wilson-type fermions, the probability of encountering an exceptional configuration is drastically increased, while for staggered fermions one approaches the dangerous low mass regime at finite lattice spacing. Apart from these technical difficulties and the need for an additional observable to fix $m_u - m_d$, however, the introduction of strong isospin splitting is straightforward.

QED, on the other hand, has a number of features that make its *ab initio* treatment more difficult. First of all, the QED coupling constant α has a pole in the UV [157] so we are dealing with an effective theory. Secondly, all electrically charged particles are no more gauge invariant. Computing propagators with the methods described in Sect. 3 will trivially give 0 unless one fixes a gauge or inserts appropriate gauge links in between source and sink to points. Furthermore, for Wilson-type fermions, there will be an additional additive mass renormalization that will be different for up and down type quarks due to their different electrical charge. Finally, QED does not have a mass gap. It, therefore, features power law finite volume effects, in contrast to QCD. One might also think that adding QED will necessitate adding electrons to the lattice theory, which would be difficult because of their very small mass. Their contribution, however, only appears at $\mathcal{O}(\alpha^2)$ compared to $\mathcal{O}(\alpha\alpha_s)$ for quarks, so they may be neglected.

One advantage of QED though is that it is an Abelian theory. However, compactifying the photon field A_μ via gauge links U_μ, as we did for the gluon field in Sect. 2.2, would introduce spurious self couplings. It is, therefore, reasonable to use a non-compact photon action, *e.g.*

$$S_\gamma = \frac{1}{2V_4} \sum_{k,\mu} \left|\hat{k}\right|^2 \left|A_\mu^k\right|^2 , \qquad \hat{k} = \frac{e^{iak_\mu} - 1}{ia} \tag{110}$$

in Feynman gauge momentum representation. Note that in Eq. (110) the prefactor of the $k = 0$ mode is 0. Therefore, A_μ^0 is not constrained and may freely fluctuate. It is also easy to check that it is both gauge invariant and not contributing to the field strength $F_{\mu\nu} = \partial_\mu A_\nu - \partial_\nu A_\mu$. Its only effect is to create a potential difference when winding around the lattice nontrivially

and returning to the same point. This is a pure lattice artefact appearing at finite volume and one should subtract it [158]. Due to the $1/2V_4$ prefactor in Eq. (110), the theory thus obtained has the same infinite volume limit.

There is a problem with this simple subtraction scheme however. Subtracting the $k = 0$ mode is equivalent to adding a term

$$\xi \sum_{\mu} \left(\sum_{x} a^4 A_\mu(x) \right)^2 \tag{111}$$

to the action and letting the Lagrange multiplier $\xi \to \infty$. Evidently, this term spoils reflection positivity as it connects all field components at points on arbitrary time slices with each other and the resulting theory is not guaranteed to possess a well-defined Hamiltonian.

This deficiency can be cured by making the Lagrange multiplier in Eq. (111) time dependent

$$\sum_{t} \eta(t) \sum_{\mu} \left(\sum_{\vec{x}} a^4 A_\mu(t, \vec{x}) \right)^2 . \tag{112}$$

With $\eta(t) \to \infty$, this is equivalent to subtracting all modes $\vec{k} = 0$ from the action, a procedure first proposed by Hayakawa and Uno [159]. Using the Hayakawa–Uno (HU) subtraction in Coulomb gauge results in a theory that is reflection positive [122]. Additionally, the HU subtraction is a pure finite volume effect. Finite volume terms are universal up to $O(1/L^2)$ and $O(1/L^3)$ terms do not diverge for infinite volume or time extent [122, 160].

It is interesting to note that although the HU subtraction is not gauge invariant, one can define a slightly modified subtraction that is gauge invariant and coincides with the HU subtraction in temporal gauge. We can define this scheme by adding to the action

$$\xi \left(\sum_{x} a^4 A_0(x) \right)^2 + \sum_{t} \eta(t) \sum_{i} \left(\sum_{\vec{x}} a^4 A_i(t, \vec{x}) \right)^2 \tag{113}$$

with $\xi, \eta(t) \to \infty$. It thus removes from the action the components A_0^0 and $\vec{A}^{(k_0, \vec{0})}$ for all k_0. With the additional $A_0^k = 0$ in temporal gauge, this new scheme is identical to HU in that gauge and, therefore, seems to fulfil reflection positivity, too.

QED and strong isospin splitting have introduced two new parameters α and $m_u - m_d$ to our lattice theory that need to be extrapolated to the physical point. We, again, would like to find two experimentally accessible

observables that are strongly dependent on α and $m_u - m_d$, and not so on other parameters. One such observable is the mass difference between charged and neutral kaons $M^2_{K^\pm} - M^2_{K^0}$. As a second observable, one can take the value of the renormalized QED coupling α itself because, in contrast to α_s of QCD, it is very small at low energies. The renormalization scheme best suited to obtain α is, in fact, provided by the gradient flow (see Eq. (99)) for photon fields.

Having defined the physical point, the target observables, which in this case are hadron isospin splittings, can be extrapolated there. Skipping further technical details that can be found in [122], the lattice predictions for some hadronic isospin splittings are displayed in the left-hand panel of Fig. 27.

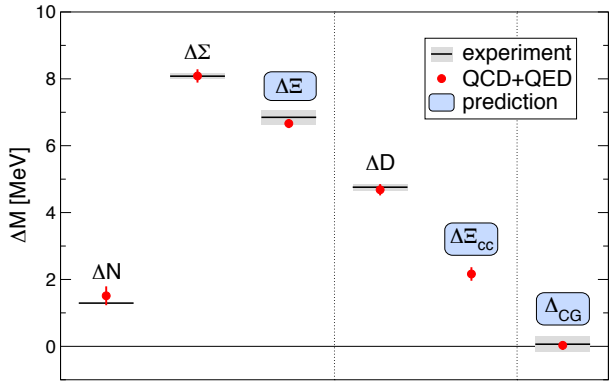

Fig. 27. Isospin splitting of some ground state hadrons from [122]. In the left-hand panel, boxes (grey) represent experimental uncertainties and dots (red) are lattice predictions. Δ_{CG} denotes the violation of the Coleman–Glashow relation [161], a quark model relation predicting $\Delta\Sigma - \Delta\Xi - \Delta N = 0$.

5. QCD thermodynamics

5.1. Formulation of QCD at finite temperature

We now turn our attention to finite temperature QCD. Introducing finite temperature into an Euclidean quantum field theory is straightforward. For a generic QFT with fields Φ and Lagrangian L, the path integral is given as the vacuum to vacuum transition amplitude

$$\mathcal{Z} = \int D\Phi e^{-\int_{-\infty}^{\infty} dtL} = \langle 0|0\rangle\,. \tag{114}$$

At finite Euclidean time extent $\mathcal{T}$ and with corresponding periodic/anti-periodic boundary conditions for bosons/fermions, one instead obtains

$$\mathcal{Z}_{\mathcal{T}} = \int D\Phi e^{-\int_0^{\mathcal{T}} dtL} = \sum_i \langle i|e^{-E_i\mathcal{T}}|i\rangle = \mathrm{Tr}\left(e^{-\mathcal{H}\mathcal{T}}\right) \tag{115}$$

which describes a thermal ensemble at a temperature $T = 1/\mathcal{T}$ given by the inverse time extent of the system.

Introducing finite temperature into a lattice theory is, therefore, achieved by simply reducing its time extent $T = aN_t$. One can vary T in steps of a which, especially at high temperatures, can be very coarse. As an alternative, one may keep the number of lattice points in the time direction N_t fixed and vary the lattice spacing a instead which can be achieved by varying the gauge coupling $\beta = 6/g^2$. The advantage of this method is that the temperature might be varied continuously, but one has to keep in mind that all other quantities vary with β, too. The spatial volume is directly affected by a change in a, and so is the relation between bare quark masses in lattice units and renormalized physical quark masses. In order to ensure that by changing β, one does not change the parameters of the theory as well, we have to determine the physical point at each β as outlined in Sect. 4.1. The resulting path through the parameter space of our theory connects parameter sets describing the same physical situation as the cutoff is varied. In the thermodynamics literature, this is known as the line of constant physics (LCP).

The LCP will, of course, depend on the specific observables chosen to identify the physical point. The difficulty of determining it also depends largely on the action used. For the $2 + 1$ flavour staggered action that is in broad use today, one of the two ratios necessary to fix the LCP is simply given by the ratio of bare quark masses m_s/m_{ud}. Although it is not an experimentally accessible quantity, it is known to a good enough accuracy and its use reduces the number of parameters that need to be independently tuned by one. For Wilson-type fermions, on the other hand, the additive quark mass renormalization renders the search for an LCP much more difficult so that it is preferable to vary the temperature by varying N_t.

As an example, Fig. 28 displays a determination of the relation between lattice spacing a and bare gauge coupling β along a LCP from a recent calculation with $2 + 1$ flavour stout-smeared staggered fermions. It is important to note, that one can define LCPs which are not physical. One can *e.g.* set the quark mass ratio m_s/m_{ud} to unphysically small values. The results obtained will be consistent, but will not describe the real physical situation.

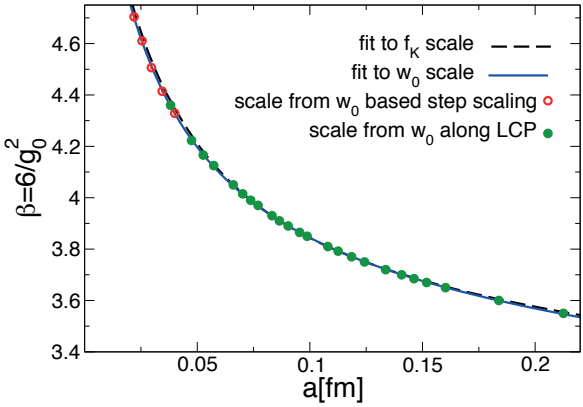

Fig. 28. Relation between bare gauge coupling and lattice spacing from [162].

5.2. Identifying phase transitions

One of the main motivations for dealing with thermodynamics is the exploration of the phase structure of a theory. Generically, phase transitions appear only in infinite volume. Studying their emergence at finite volume is best achieved by finite size scaling techniques.

In QCD, we can define the chiral susceptibility as the second derivative of the partition function with respect to the (light) quark mass

$$\chi_{\bar{\psi}\psi} = \frac{T}{V}\frac{\partial^2 \mathcal{Z}}{\partial m^2} = \frac{\partial \langle \bar{\psi}\psi \rangle}{\partial m} \,. \tag{116}$$

The corresponding quantity in pure gauge theory, the Polyakov loop susceptibility, is plotted in the left-hand panel of Fig. 29 *versus* β for three different lattice volumes. It is clearly visible that the peak height scales with volume,

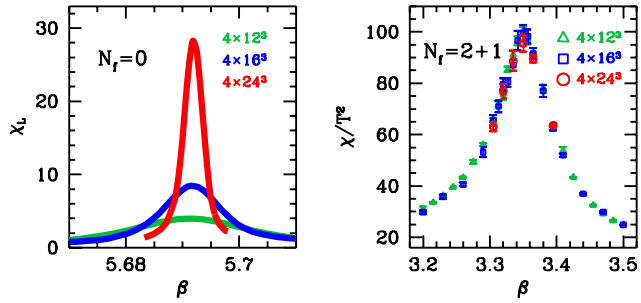

Fig. 29. Polyakov loop susceptibility in pure SU(3) gauge theory (left-hand panel) and chiral susceptibility of $2+1$ flavour QCD (right-hand panel) *versus* β from [10, 163].

which is a sign for a phase transition that develops in the infinite volume limit. The exponent with which the peak height diverges with volume depends on the universality class. In the present case, the height scales $\propto V$, which is characteristic of a first order phase transition.

In one of the landmark calculations of lattice QCD [163], it was demonstrated that at physical quark masses (and vanishing chemical potential) QCD does not exhibit a phase transition but rather a crossover. In the right-hand panel of Fig. 29, the chiral susceptibility is plotted *versus* β for the same three lattice volumes as in the pure gauge theory case. In contrast to pure gauge theory, the peak does not show an increase with volume though.

As clear as this evidence might seam, it is not conclusive yet because it lacks a proper continuum limit. The calculation was, therefore, repeated for 4 different values of N_t, which allowed for taking the continuum limit of the peak height (upper panel of Fig. 30) before extrapolating it to infinite volume (lower panel of Fig. 30). The result clearly shows that the peak height does not diverge and that therefore QCD has no phase transition at vanishing chemical potential.

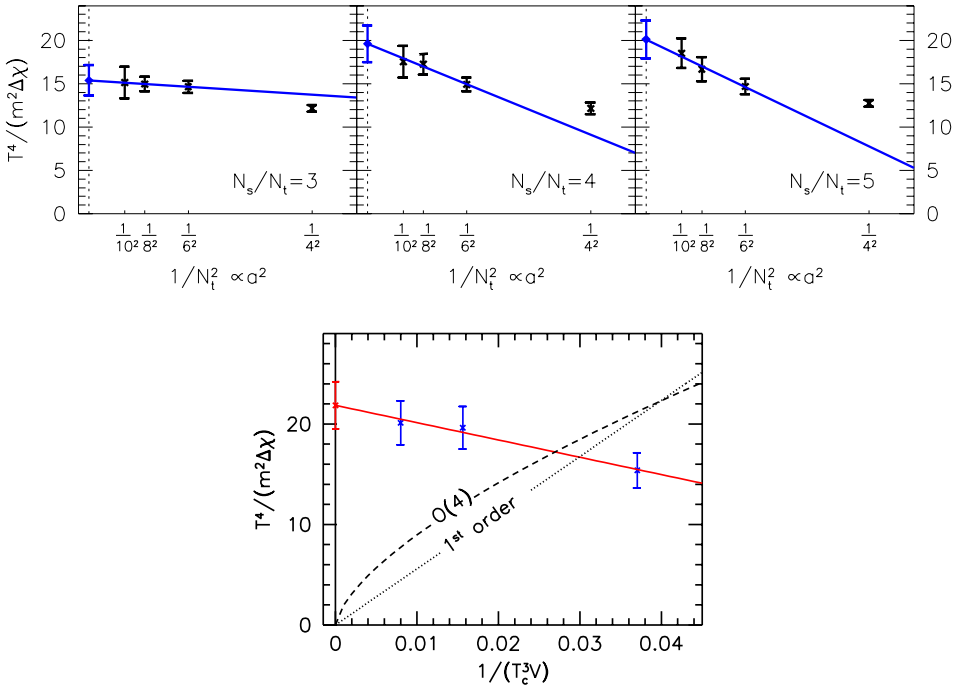

Fig. 30. Continuum extrapolation of the peak height for 3 different lattice volumes (upper panel) and infinite volume behaviour of the inverse peak height (lower panel) from [163].

5.3. Critical and pseudocritical temperatures

As we have seen now that QCD does not exhibit a phase transition, the question about its critical temperature is moot: there simply is no critical temperature. One might nonetheless be interested in finding the temperature where the thermodynamic observables exhibit the largest change, *e.g.* where the peak in the chiral susceptibility is located even if it does not diverge.

It is evident that there is no unique pseudocritical temperature. As a simple illustration, we might look at the phase diagram of water (Fig. 31). Let us assume we want to determine the transition temperature of water at constant pressure below the critical point. We could *e.g.* measure the density ρ or the specific heat c_p for different temperatures. The critical temperature will be the unique point where ρ is discontinuous and c_p diverges and redefining our observables by multiplying them with a smooth function of T, *e.g.* T^2 will not change the situation (lower left-hand panel of Fig. 31). If, on the other hand, the pressure is above the critical value, not only will the peak of c_p generically be at a different temperature than the largest change in ρ, but redefining the observables by multiplying them with T^2 will shift those temperatures (upper left panel of Fig. 31).

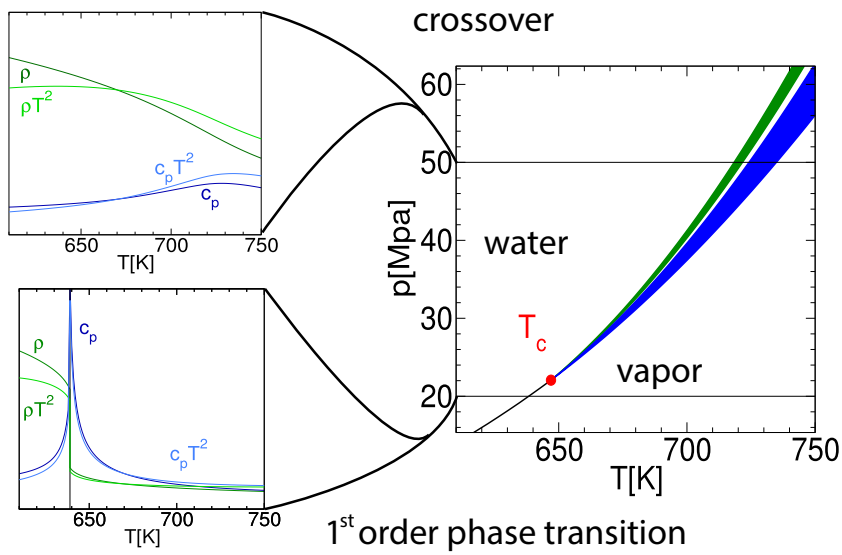

Fig. 31. Illustration of the phase diagram of water. In the right-hand panel the phase structure is plotted in the p *versus* T plane, the left-hand panels show the temperature dependence of the density ρ and the specific heat c_p *versus* temperature at a line of constant pressure below and above the critical point.

In QCD, a pseudocritical temperature may also be computed for different observables. In addition to the chiral susceptibility (Eq. (116)), quark number susceptibilities

$$\chi_2^q = \frac{T}{V} \left. \frac{\partial^2 \mathcal{Z}_\mu}{\partial \mu_q^2} \right|_{\mu_q=0} \tag{117}$$

may be used. One may also use the renormalized chiral condensate

$$\langle \bar{\psi}\psi \rangle_R = \frac{m_{ud}}{M_\pi^4} \left(\langle \bar{\psi}\psi \rangle_{ud} - \langle \bar{\psi}\psi \rangle_{ud,T} \right) \tag{118}$$

itself or a quantity called the strange subtracted chiral condensate that is defined as

$$\Delta_{l,s} = \frac{\langle \bar{\psi}\psi \rangle_{ud,T} - \frac{m_{ud}}{m_s} \langle \bar{\psi}\psi \rangle_{s,T}}{\langle \bar{\psi}\psi \rangle_{ud} - \frac{m_{ud}}{m_s} \langle \bar{\psi}\psi \rangle_{s}} , \tag{119}$$

where $\langle \bar{\psi}\psi \rangle_{q,T}$ is the chiral condensate for quark flavour q at temperature T and $\langle \bar{\psi}\psi \rangle_q$ the corresponding condensate at zero temperature.

In Fig. 32, the behaviour of three of these observables is plotted. The pseudocritical temperature extracted is in the range of $T_c \sim 145$–165 MeV. These results are in agreement with older results from the Wuppertal–Budapest Collaboration [165, 166]. They are also in agreement with recent results of the hotQCD Collaboration [167] that had previously quoted substantially higher numbers [168] (see Fig. 33).

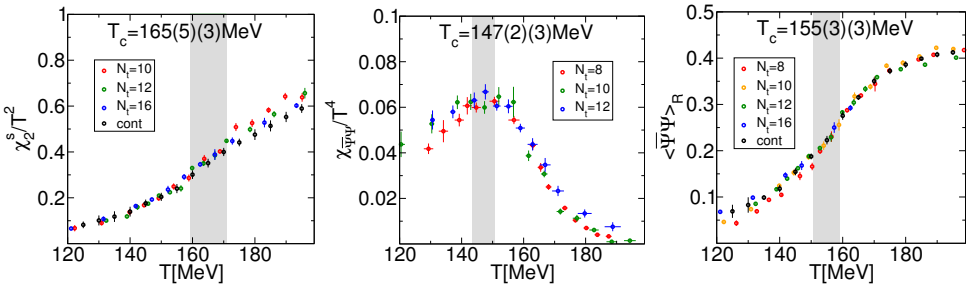

Fig. 32. Determination of the pseudocritical temperature of QCD from 3 different observables from [164].

Some valuable crosschecks of the results on the phase transition are beginning to emerge from lattice calculations with alternative fermion formulations. Although continuum results at physical quark masses are currently only available for staggered fermions due to their relatively low computational cost, there are results at larger quark masses from Wilson and overlap

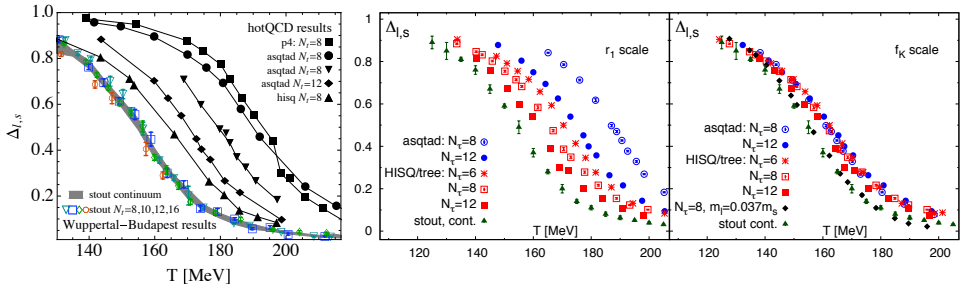

Fig. 33. Comparison of the strange subtracted chiral condensate of the Wupertal–Budapest Collaboration (stout) and the hotQCD Collaboration (p4, asqtad and hisq actions) as presented by the Wuppertal–Budapest Collaborations (left-hand panel, [164]) and the hotQCD Collaboration (central and right-hand panels, [167]). Note that unless otherwise noted, hotQCD results are for an unphysical quark mass ratio $m_s/m_{ud} = 20$.

fermions [169–171]. As an example, Fig. 34 shows a comparison of the staggered and Wilson chiral condensate at an unphysically large pion mass. As one can see, the continuum results are in nice agreement.

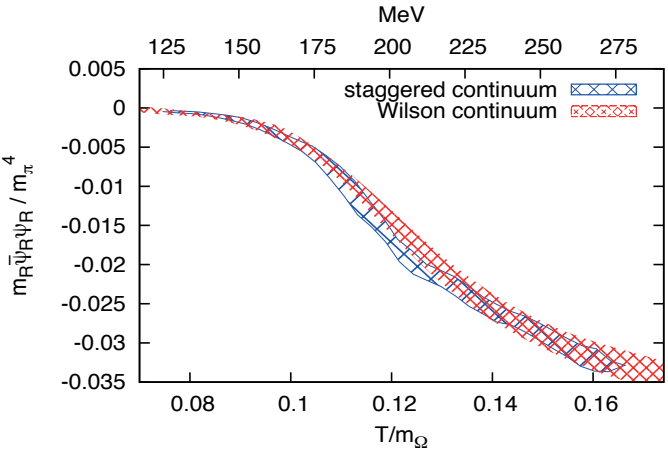

Fig. 34. Comparison of the continuum extracted renormalized chiral condensate (Eq. (118)) obtained from staggered and Wilson fermions at an unphysically large $M_\pi \approx 545$ MeV [170].

5.4. Equation of state

The final lattice calculation I want to briefly discuss is the QCD equation of state. From standard thermodynamic relations, we find that up to finite volume corrections the pressure is given by

$$p^{\mathrm{lat}}(\beta, m_q) = \frac{Ta^4}{V} \ln \mathcal{Z}(\beta, m_q)\,. \tag{120}$$

Since lattice QCD does not give us the normalization of the partition function, Eq. (120) can only be used to compute pressure differences

$$p^{\mathrm{lat}}(\beta, m_q) - p^{\mathrm{lat}}\left(\beta^0, m_q^0\right) = \frac{Ta^4}{V} \int\limits_{\left(\beta^0, m_q^0\right)}^{(\beta, m_q)} \frac{\partial \ln \mathcal{Z}}{\partial \beta'} d\beta' \frac{\partial \ln \mathcal{Z}}{\partial m_q'} dm_q'\,. \tag{121}$$

It is important to note that the pressure difference in Eq. (121) is independent of the integration path, which allows one to choose optimal integration paths dependent on the problem. The derivatives of the partition function occurring in Eq. (121) are the gauge action and the chiral condensate

$$\frac{\partial \ln \mathcal{Z}}{\partial \beta} = -\langle S_G \rangle\,, \qquad \frac{\partial \ln \mathcal{Z}}{\partial m_q} = \left\langle \bar{\psi}\psi \right\rangle_q\,. \tag{122}$$

Like in the previous section, a $T = 0$ subtraction has to be performed on them to remove divergences.

We can now integrate the pressure starting from a reference point. One straightforward method to do so is to compute the derivative of the pressure with respect to temperature along the LCP. The temperature derivative of the pressure is related to the trace anomaly

$$I = \Theta^{\mu\mu} = \epsilon - 3p \tag{123}$$

via the relation

$$\frac{I}{T^4} = T \frac{\partial}{\partial T} \frac{p(T)}{T^4}\,. \tag{124}$$

Alternatively, one can construct the pressure as a function of β and the quark masses, constraining its form by computing derivatives with respect to all these parameters [172].

There are also different possible choices for a reference point. Ideally, the pressure should be negligible at the reference point. One natural choice is *e.g.* a physical point at low temperature. The pressure will be low at low temperature and, in addition, it can be estimated rather accurately in the hadron resonance gas model [174–176]. However, in a fixed N_t approach,

the lattice spacing $a = N_t/T$ increases dramatically at low T and there are potentially large discretization effects. Alternatively, one may choose a reference point that is not on the LCP. Increasing the bare quark masses at a fixed β leads to an unphysical theory deeply in the confined phase where the pressure is almost zero which can serve as an ideal reference point [162]. In the left-hand panel of Fig. 35, the result of a pressure integration from such a reference point are displayed for two lattice spacings.

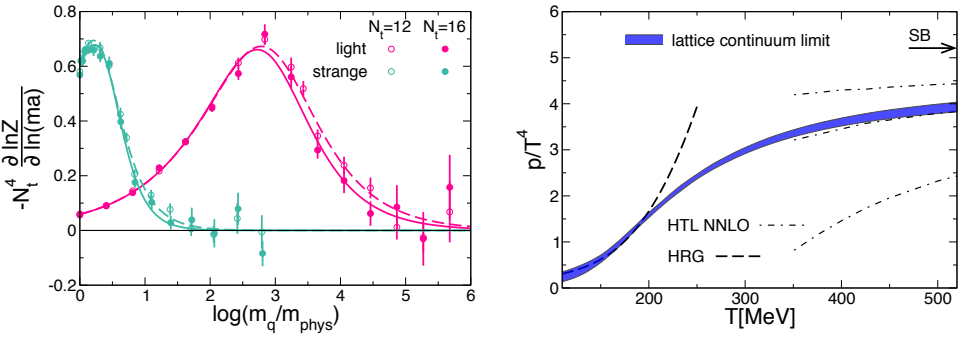

Fig. 35. Pressure integration from a reference point at high bare quark mass for two N_t (left-hand panel) and the continuum extrapolated pressure as a function of temperature (right-hand panel) from [162]. The β of the reference point corresponds to $T \sim 214$ MeV at the physical point. In the right-hand panel, HRG denotes the hadron resonance gas result and HTL refers to the hard thermal loop result of [173].

In the right-hand panel of Fig. 35, the continuum extrapolated pressure is plotted *versus* temperature and compared to the hadron resonance gas prediction, the hard thermal loop prediction and the Stefan–Boltzmann limit. Further thermodynamic quantities can be obtained from $p(T)$. Apart from the trace anomaly (Eq. (124)), we can compute the energy density ϵ, the entropy density s and the speed of sound c_s via

$$\epsilon = I + 3p\,, \qquad s = \frac{1}{T}(\epsilon + p)\,, \qquad c_s^2 = \frac{\partial p}{\partial \epsilon}\,. \tag{125}$$

Similarly to the case of the pseudocritical temperature discussed in Sect. 5.3, there has been until very recently a marked discrepancy in the literature regarding the equation of state as obtained by the two major collaborations computing it. The peak height of the trace anomaly reported by the hotQCD Collaboration [179, 180] was substantially larger than that reported by the Wuppertal–Budapest Collaboration [162, 172]. With the latest results of the hotQCD Collaboration [177], this discrepancy has disappeared and there is now consensus on the on the QCD equation of state at vanishing chemical potential (see Fig. 36).

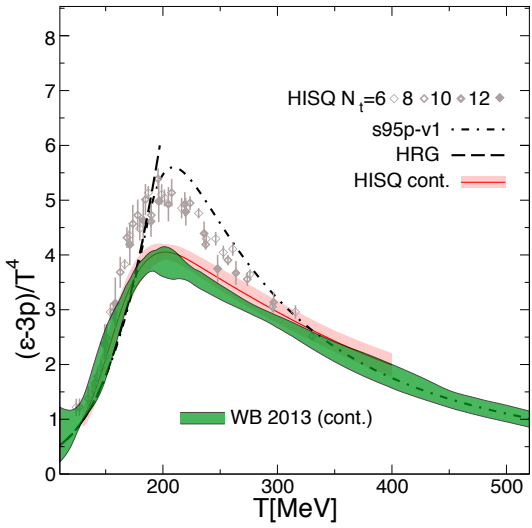

Fig. 36. Trace anomaly *versus* temperature from the Wuppertal–Budapest Collaboration [162] and the hotQCD Collaboration [177]. The "s95p-v1" parametrisation [178] and a previous hotQCD result (HISQ, [179]) is plotted for comparison.

I would like to thank Stephan Dürr, Zoltan Fodor, Sandor Katz, Laurent Lellouch and Kalman Szabo for discussions and support in preparing the lectures.

REFERENCES

[1] H. Fritzsch, M. Gell-Mann, H. Leutwyler, *Phys. Lett.* **B47**, 365 (1973).

[2] H.D. Politzer, *Phys. Rev. Lett.* **30**, 1346 (1973).

[3] D.J. Gross, F. Wilczek, *Phys. Rev. Lett.* **30**, 1343 (1973).

[4] M. Creutz, *Quarks, Gluons and Lattices*, Cambridge Univ. Press, Cambridge 1984.

[5] I. Montvay, G. Munster, *Quantum Fields on a Lattice*, Cambridge Univ. Press, 1994 (Cambridge Monographs on Mathematical Physics).

[6] R. Gupta, `arXiv:hep-lat/9807028`.

[7] J. Smit, *Introduction to Quantum Fields on a Lattice: A Robust Mate*, Cambridge Univ. Press, Cambridge 2002.

[8] H.J. Rothe, *Lattice Gauge Theories: An Introduction*, World Scientific, Singapore 2005.

[9] T. DeGrand, C.E. Detar, *Lattice Methods for Quantum Chromodynamics*, World Scientific, Singapore 2006.

[10] Z. Fodor, S.D. Katz, arXiv:0908.3341 [hep-ph].
[11] Ch. Gattringer, Ch.B. Lang, *Quantum Chromodynamics on the Lattice*, Springer, Berlin 2010.
[12] Z. Fodor, Ch. Hoelbling, *Rev. Mod. Phys.* **84**, 449 (2012).
[13] S.L. Adler, *Phys. Rev.* **177**, 2426 (1969).
[14] J.S. Bell, R. Jackiw, *Nuovo Cim.* **A60**, 47 (1969).
[15] K.G. Wilson, *Phys. Rev.* **D10**, 2445 (1974).
[16] G. Curci, P. Menotti, G. Paffuti, *Phys. Lett.* **B130**, 205 (1983).
[17] M. Luscher, P. Weisz, *Commun. Math. Phys.* **97**, 59 (1985).
[18] M. Luscher, P. Weisz, *Commun. Math. Phys.* **98**, 433 (1985).
[19] M. Luscher, P. Weisz, *Phys. Lett.* **B158**, 250 (1985).
[20] Y. Iwasaki, preprint UTHEP-118, 1983.
[21] T. Takaishi, *Phys. Rev.* **D54**, 1050 (1996).
[22] P. de Forcrand *et al.*, *Nucl. Phys.* **B577**, 263 (2000).
[23] K. Symanzik, *Nucl. Phys.* **B226**, 187 (1983).
[24] K. Symanzik, *Nucl. Phys.* **B226**, 205 (1983).
[25] H.B. Nielsen, M. Ninomiya, *Nucl. Phys.* **B185**, 20 (1981).
[26] H.B. Nielsen, M. Ninomiya, *Nucl. Phys.* **B193**, 173 (1981).
[27] H.B. Nielsen, M. Ninomiya, *Phys. Lett.* **B105**, 219 (1981).
[28] L.H. Karsten, J. Smit, *Nucl. Phys.* **B183**, 103 (1981).
[29] A. Chodos, J.B. Healy, *Phys. Rev.* **D16**, 387 (1977).
[30] W. Kerler, *Phys. Rev.* **D23**, 2384 (1981).
[31] K.G. Wilson, *New Phenomena in Subnuclear Physics. Part A*, Proceedings of the First Half of the 1975 International School of Subnuclear Physics, Erice, Sicily, July 11–August 1, 1975, ed. A. Zichichi, Plenum Press, New York, 1977, p. 69, CLNS-321.
[32] M.F. Atiyah, I.M. Singer, *Ann. Math.* **87**, 546 (1968).
[33] H.W. Hamber, Chi Min Wu, *Phys. Lett.* **B133**, 351 (1983).
[34] B. Sheikholeslami, R. Wohlert, *Nucl. Phys.* **B259**, 572 (1985).
[35] R. Wohlert, Preprint DESY 87/069, 1987.
[36] M. Luscher, P. Weisz, *Nucl. Phys.* **B479**, 429 (1996).
[37] M. Luscher *et al.*, *Nucl. Phys.* **B491**, 323 (1997).
[38] S. Capitani, S. Dürr, Ch. Hoelbling, *J. High Energy Phys.* **11**, 028 (2006).
[39] J.B. Kogut, L. Susskind, *Phys. Rev.* **D11**, 395 (1975).
[40] T. Banks, L. Susskind, J.B. Kogut, *Phys. Rev.* **D13**, 1043 (1976).
[41] L. Susskind, *Phys. Rev.* **D16**, 3031 (1977).
[42] J. Smit, J.C. Vink, *Nucl. Phys.* **B286**, 485 (1987).
[43] D.H. Adams, *Phys. Rev.* **D72**, 114512 (2005).

[44] S. Dürr, Ch. Hoelbling, *Phys. Rev.* **D71**, 054501 (2005).
[45] C. Bernard, *Phys. Rev.* **D73**, 114503 (2006).
[46] C. Bernard, C.E. DeTar, Z. Fu, S. Prelovsek, *Phys. Rev.* **D76**, 094504 (2007).
[47] S. Prelovsek, *Phys. Rev.* **D73**, 014506 (2006).
[48] S. Dürr, Ch. Hoelbling, U. Wenger, *Phys. Rev.* **D70**, 094502 (2004).
[49] S. Dürr, Ch. Hoelbling, *Phys. Rev.* **D69**, 034503 (2004).
[50] C.T.H. Davies *et al.*, *Phys. Rev. Lett.* **92**, 022001 (2004).
[51] C.T.H. Davies, G.P. Lepage, F. Niedermayer, D. Toussaint, *Nucl. Phys. Proc. Suppl.* **140**, 261 (2005).
[52] C. Aubin *et al.*, *Phys. Rev.* **D70**, 114501 (2004).
[53] E. Follana, C.T.H. Davies, G.P. Lepage, J. Shigemitsu, *Phys. Rev. Lett.* **100**, 062002 (2008).
[54] A. Bazavov *et al.*, *Phys. Rev.* **D82**, 074501 (2010).
[55] A. Bazavov *et al.*, *Rev. Mod. Phys.* **82**, 1349 (2010).
[56] C. Bernard, M. Golterman, Y. Shamir, *Phys. Rev.* **D73**, 114511 (2006).
[57] J. Giedt, *Nucl. Phys.* **B782**, 134 (2007).
[58] C. Bernard, M. Golterman, Y. Shamir, *Phys. Rev.* **D77**, 074505 (2008).
[59] Y. Shamir, *Phys. Rev.* **D75**, 054503 (2007).
[60] C. Bernard, *Phys. Rev.* **D71**, 094020 (2005).
[61] S. Dürr, Ch. Hoelbling, *Phys. Rev.* **D74**, 014513 (2006).
[62] M. Creutz, *Phys. Lett.* **B649**, 230 (2007).
[63] C. Bernard, M. Golterman, Y. Shamir, S.R. Sharpe, *Phys. Lett.* **B649**, 235 (2007).
[64] A. Hasenfratz, R. Hoffmann, *Phys. Rev.* **D74**, 014511 (2006).
[65] M. Creutz, *Phys. Lett.* **B649**, 241 (2007) [rebuttal to `arXiv:hep-lat/0603027`].
[66] S. Dürr, *PoS* **LAT2005**, 021 (2006).
[67] S.R. Sharpe, *PoS* **LAT2006**, 022 (2006).
[68] S. Dürr, *Phys. Rev.* **D85**, 114503 (2012).
[69] R. Frezzotti, P.A. Grassi, S. Sint, P. Weisz, *J. High Energy Phys.* **08**, 058 (2001).
[70] L.H. Karsten, *Phys. Lett.* **B104**, 315 (1981).
[71] F. Wilczek, *Phys. Rev. Lett.* **59**, 2397 (1987).
[72] M. Creutz, *J. High Energy Phys.* **04**, 017 (2008).
[73] A. Borici, *Phys. Rev.* **D78**, 074504 (2008).
[74] D.H. Adams, *Phys. Lett.* **B699**, 394 (2011) [`arXiv:1008.2833 [hep-lat]`].
[75] P. de Forcrand, A. Kurkela, M. Panero, *PoS* **LATTICE2010**, 080 (2010) [`arXiv:1102.1000 [hep-lat]`].

[76] Ch. Hoelbling, *Phys. Lett.* **B696**, 422 (2011).
[77] P.H. Ginsparg, K.G. Wilson, *Phys. Rev.* **D25**, 2649 (1982).
[78] P. Hasenfratz, F. Niedermayer, *Nucl. Phys.* **B414**, 785 (1994).
[79] T.A. DeGrand, A. Hasenfratz, P. Hasenfratz, F. Niedermayer, *Nucl. Phys.* **B454**, 587 (1995).
[80] W. Bietenholz, U.J. Wiese, *Nucl. Phys.* **B464**, 319 (1996).
[81] P. Hasenfratz, V. Laliena, F. Niedermayer, *Phys. Lett.* **B427**, 125 (1998).
[82] C.G. Callan Jr., J.A. Harvey, *Nucl. Phys.* **B250**, 427 (1985).
[83] S.A. Frolov, A.A. Slavnov, *Phys. Lett.* **B309**, 344 (1993).
[84] D.B. Kaplan, *Phys. Lett.* **B288**, 342 (1992).
[85] Y. Shamir, *Nucl. Phys.* **B406**, 90 (1993).
[86] R. Narayanan, H. Neuberger, *Phys. Lett.* **B302**, 62 (1993).
[87] R. Narayanan, H. Neuberger, *Nucl. Phys.* **B412**, 574 (1994).
[88] R. Narayanan, H. Neuberger, *Phys. Rev. Lett.* **71**, 3251 (1993).
[89] R. Narayanan, H. Neuberger, *Nucl. Phys.* **B443**, 305 (1995).
[90] H. Neuberger, *Phys. Lett.* **B417**, 141 (1998).
[91] H. Neuberger, *Phys. Lett.* **B427**, 353 (1998).
[92] M. Luscher, *Phys. Lett.* **B428**, 342 (1998).
[93] I. Horvath, *Phys. Rev. Lett.* **81**, 4063 (1998).
[94] W. Bietenholz, `arXiv:hep-lat/9901005 [hep-lat]`.
[95] M. Albanese *et al.*, *Phys. Lett.* **B192**, 163 (1987).
[96] C. Morningstar, M.J. Peardon, *Phys. Rev.* **D69**, 054501 (2004).
[97] A. Hasenfratz, F. Knechtli, *Phys. Rev.* **D64**, 034504 (2001).
[98] S. Dürr, G. Koutsou, *Phys. Rev.* **D83**, 114512 (2011) [`arXiv:1012.3615 [hep-lat]`].
[99] S. Dürr, *Phys. Rev.* **D87**, 114501 (2013).
[100] C.W. Bernard, T.A. DeGrand, *Nucl. Phys. Proc. Suppl.* **B83**, 845 (2000).
[101] S. Dürr *et al.*, *Science* **322**, 1224 (2008).
[102] N. Metropolis *et al.*, *J. Chem. Phys.* **21**, 1087 (1953).
[103] D.J.E. Callaway, A. Rahman, *Phys. Rev. Lett.* **49**, 613 (1982).
[104] D.J.E. Callaway, A. Rahman, *Phys. Rev.* **D28**, 1506 (1983).
[105] J. Polonyi, H.W. Wyld, *Phys. Rev. Lett.* **51**, 2257 (1983).
[106] G.G. Batrouni *et al.*, *Phys. Rev.* **D32**, 2736 (1985).
[107] S. Duane, *Nucl. Phys.* **B257**, 652 (1985).
[108] S. Duane, J.B. Kogut, *Phys. Rev. Lett.* **55**, 2774 (1985).
[109] S. Duane, J.B. Kogut, *Nucl. Phys.* **B275**, 398 (1986).
[110] S. Duane, A.D. Kennedy, B.J. Pendleton, D. Roweth, *Phys. Lett.* **B195**, 216 (1987).

[111] D.H. Weingarten, D.N. Petcher, *Phys. Lett.* **B99**, 333 (1981).
[112] E. Marinari, G. Parisi, C. Rebbi, *Nucl. Phys.* **B190**, 734 (1981).
[113] S. Dürr, Z. Fodor, Ch. Hoelbling, T. Kurth, *J. High Energy Phys.* **04**, 055 (2007).
[114] S. Dürr *et al.*, *J. High Energy Phys.* **1108**, 148 (2011) [arXiv:1011.2711 [hep-lat]].
[115] S. Schaefer, R. Sommer, F. Virotta, *PoS* **LAT2009**, 032 (2009).
[116] Z. Fodor, S.D. Katz, K.K. Szabo, *J. High Energy Phys.* **08**, 003 (2004).
[117] T.A. DeGrand, S. Schaefer, *Phys. Rev.* **D71**, 034507 (2005).
[118] N. Cundy *et al.*, *Comput. Phys. Commun.* **180**, 26 (2009).
[119] G.I. Egri, Z. Fodor, S.D. Katz, K.K. Szabo, *J. High Energy Phys.* **0601**, 049 (2006).
[120] S. Hashimoto *et al.*, *PoS* **LAT2006**, 052 (2006).
[121] M. Luscher, S. Schaefer, *J. High Energy Phys.* **1107**, 036 (2011).
[122] Sz. Borsanyi *et al.*, arXiv:1406.4088 [hep- lat].
[123] M. Gell-Mann, R.J. Oakes, B. Renner, *Phys. Rev.* **175**, 2195 (1968).
[124] Ch. Hoelbling, *PoS* **LATTICE2010**, 011 (2010).
[125] B. Blossier *et al.*, *J. High Energy Phys.* **07**, 043 (2009).
[126] R. Baron *et al.*, *PoS* **LAT2010**, 123 (2010).
[127] G. Schierholz, private communication, 2010.
[128] W. Bietenholz *et al.*, arXiv:1012.4371 [hep-lat].
[129] S. Aoki *et al.*, *Phys. Rev.* **D81**, 074503 (2010).
[130] S. Aoki *et al.*, *Phys. Rev.* **D79**, 034503 (2009).
[131] Y. Aoki *et al.* [RBC and UKQCD collaborations], *Phys. Rev.* **D83**, 074508 (2011) [arXiv:1011.0892 [hep-lat]].
[132] R. Mawhinney, private communication, 2010.
[133] J. Noaki *et al.*, *PoS* **LAT2009**, 096 (2009).
[134] Huey-Wen Lin *et al.*, *Phys. Rev.* **D79**, 034502 (2009).
[135] G.P. Engel *et al.*, *Phys. Rev.* **D82**, 034505 (2010).
[136] B.B. Brandt *et al.*, *PoS* **LATTICE2010**, 164 (2010).
[137] G. Colangelo, S. Dürr, Ch. Haefeli, *Nucl. Phys.* **B721**, 136 (2005).
[138] Ch. Michael, *Nucl. Phys.* **B259**, 58 (1985).
[139] M. Luscher, U. Wolff, *Nucl. Phys.* **B339**, 222 (1990).
[140] R. Sommer, *Nucl. Phys.* **B411**, 839 (1994).
[141] M. Luscher, *J. High Energy Phys.* **1008**, 071 (2010).
[142] S. Borsanyi *et al.*, *J. High Energy Phys.* **1209**, 010 (2012).
[143] R. Narayanan, H. Neuberger, *J. High Energy Phys.* **0603**, 064 (2006).
[144] G. Colangelo, A. Fuhrer, Ch. Haefeli, *Nucl. Phys. Proc. Suppl.* **153**, 41 (2006).

[145] M. Luscher, *Commun. Math. Phys.* **104**, 177 (1986).
[146] J. Gasser, H. Leutwyler, *Phys. Lett.* **B184**, 83 (1987).
[147] J. Gasser, H. Leutwyler, *Phys. Lett.* **B188**, 477 (1987).
[148] J. Gasser, H. Leutwyler, *Nucl. Phys.* **B307**, 763 (1988).
[149] G. Colangelo, S. Dürr, *Eur. Phys. J.* **C33**, 543 (2004).
[150] G. Colangelo, A. Fuhrer, S. Lanz, *Phys. Rev.* **D82**, 034506 (2010).
[151] M. Luscher, *Commun. Math. Phys.* **105**, 153 (1986).
[152] M. Luscher, *Nucl. Phys.* **B354**, 531 (1991).
[153] M. Luscher, *Nucl. Phys.* **B364**, 237 (1991).
[154] K. Rummukainen, S.A. Gottlieb, *Nucl. Phys.* **B450**, 397 (1995).
[155] P. Langacker, H. Pagels, *Phys. Rev.* **D10**, 2904 (1974).
[156] H. Akaike, *IEEE Trans. Autom. Control* **19**, 716 (1974).
[157] L.D. Landau, in: *Niels Bohr and the Development of Physics*, Pergamon Press, London 1955.
[158] A. Duncan, E. Eichten, H. Thacker, *Phys. Rev. Lett.* **76**, 3894 (1996).
[159] M. Hayakawa, S. Uno, *Prog. Theor. Phys.* **120**, 413 (2008).
[160] Z. Davoudi, M.J. Savage, *Phys. Rev.* **D90**, 054503 (2014).
[161] S. Coleman, S.L. Glashow, *Phys. Rev. Lett.* **6**, 423 (1961).
[162] S. Borsanyi *et al.*, *Phys. Lett.* **B730**, 99 (2014).
[163] Y. Aoki *et al.*, *Nature* **443**, 675 (2006).
[164] S. Borsanyi *et al.*, *J. High Energy Phys.* **09**, 073 (2010).
[165] Y. Aoki, Z. Fodor, S.D. Katz, K.K. Szabo, *Phys. Lett.* **B643**, 46 (2006).
[166] Y. Aoki *et al.*, *J. High Energy Phys.* **0906**, 088 (2009).
[167] A. Bazavov *et al.*, *Phys. Rev.* **D85**, 054503 (2012).
[168] M. Cheng *et al.*, *Phys. Rev.* **D74**, 054507 (2006).
[169] T. Umeda *et al.*, *Phys. Rev.* **D85**, 094508 (2012).
[170] S. Borsanyi *et al.*, *J. High Energy Phys.* **1208**, 126 (2012).
[171] S. Borsanyi *et al.*, *Phys. Lett.* **B713**, 342 (2012).
[172] S. Borsanyi *et al.*, *J. High Energy Phys.* **1011**, 077 (2010).
[173] J.O. Andersen, L.E. Leganger, M. Strickland, N. Su, *J. High Energy Phys.* **1108**, 053 (2011).
[174] F. Karsch, K. Redlich, A. Tawfik, *Eur. Phys. J.* **C29**, 549 (2003).
[175] F. Karsch, K. Redlich, A. Tawfik, *Phys. Lett.* **B571**, 67 (2003).
[176] A. Tawfik, *Phys. Rev.* **D71**, 054502 (2005).
[177] A. Bazavov *et al.* [HotQCD Collaboration], `arXiv:1407.6387 [hep-lat]`.
[178] P. Huovinen, P. Petreczky, *Nucl. Phys.* **A837**, 26 (2010).
[179] P. Petreczky, *PoS* **LATTICE2012**, 069 (2012).
[180] A. Bazavov *et al.*, *Phys. Rev.* **D80**, 014504 (2009).